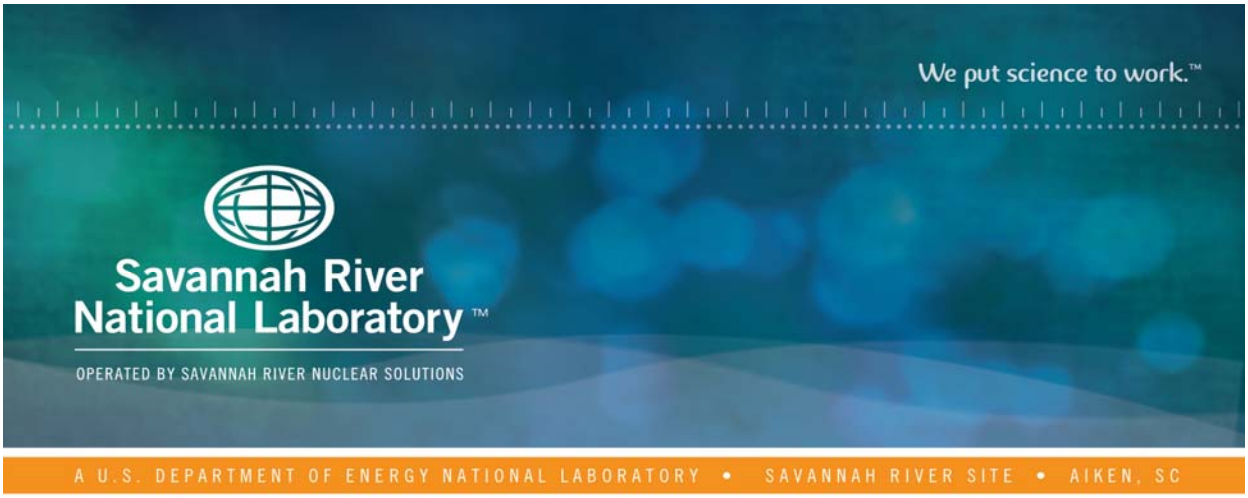

Characterization of Basin Concrete in Support of Structural Integrity Demonstration for Extended Storage

A. J. Duncan

September 2014

SRNL-STI-2014-00364, Revision 0

DISCLAIMER

Printed in the United States of America

Prepared for
U.S. Department of Energy

SRNL-STI-2014-00364

Revision 0

Keywords: ***Concrete, Mechanical Properties, Environmental Degradation, Microstructure***

Retention: *Permanent*

Characterization of Basin Concrete in Support of Structural Integrity Demonstration for Extended Storage

A. J. Duncan

September 2014

Savannah River National Laboratory™

OPERATED BY SAVANNAH RIVER NUCLEAR SOLUTIONS

Prepared for the U.S. Department of Energy under contract number DE-AC09-08SR22470.

REVIEWS AND APPROVALS

AUTHORS:

_____

A. J. Duncan, Author Date
Materials Science & Technology, Savannah River National Laboratory

TECHNICAL REVIEW:

_____

Marissa M. Reigel, Engineering Process Development Date

_____

D.L. Speed, Spent Fuel Project Engineering Date

APPROVAL:

_____

M.A. Hromyak, AMCAP SFPE Lead Date
Spent Fuel Project Engineering, M&O Engineering

_____

R.L. Sindelar, AMCAP Technical Lead Date
Materials Science & Technology, Savannah River National Laboratory

_____

K.E. Zeigler, Director Date
Materials Science & Technology, Savannah River National Laboratory

_____

M.D. Shaffer, Manager Date
Spent Fuel Project Engineering, M&O Engineering

ACKNOWLEDGEMENTS

Much of the experimental analysis was conducted by staff members at SRNL. Their assistance is gratefully acknowledged. Sectioning of the cores was performed by James Wilderman. Mounting, polishing and photography were conducted with the aid of Gregg Creech, Thaddeus Reown and Vickie Timmerman. Henry Ajo performed the SEM microanalysis. Charles Coleman, Tom White and Mark Jones dissolved and analyzed the samples using ICP-ES and IC. David Best performed Leco carbon/sulfur (C/S) analysis to determine the levels of carbon and sulfur in the concrete. David Missimer analyzed samples using X-ray Diffraction. David and Cecilia Diprete assisted in obtaining radionuclide levels in the concrete.

EXECUTIVE SUMMARY

Concrete core samples from C basin were characterized through material testing and analysis to verify the design inputs for structural analysis of the L Basin and to evaluate the type and extent of changes in the material condition of the concrete under extended service for fuel storage. To avoid the impact on operations, core samples were not collected from L area, but rather, several concrete core samples were taken from the C Basin prior to its closure. C basin was selected due to its similar environmental exposure and service history compared to L Basin.

The microstructure and chemical composition of the concrete exposed to the water was profiled from the water surface into the wall to evaluate the impact and extent of exposure. No significant leaching of concrete components was observed. Ingress of carbonation or deleterious species was determined to be insignificant. No evidence of alkali-silica reactions (ASR) was observed.

Ettringite was observed to form throughout the structure (in air voids or pores); however, the sulfur content was measured to be consistent with the initial concrete that was used to construct the facility. Similar ettringite trends were observed in the interior segments of the core samples.

The compressive strength of the concrete at the mid-wall of the basin was measured, and similar microstructural analysis was conducted on these materials post compression testing. The microstructure was determined to be similar to near-surface segments of the core samples. The average strength was 4148 psi, which is well-above the design strength of 2500 psi. The analyses showed that phase alterations and minor cracking in a microstructure did not affect the design specification for the concrete.

The following are path forward recommendations:

- Formally evaluate the concrete material and service conditions from P-reactor building concrete test results, and their applicability to L Basin concrete. A follow-up of recommended prescriptive verification tests and, if warranted, post comparisons should be performed.
- Evaluate the soil adjacent to the L Basin for sulfate content and evaluate the results for potential degradation of the concrete in contact with groundwater.
- Evaluate the potential loss of function due to aging of each of the waterstop materials in L Basin at or near the established existing or historical leak sites.
- Acquire non-radiological concrete samples at or adjacent to moist or historical leak sites be analyze for extent of degradation and grade for deleterious species infiltration potential.
- Non-destructive examination (NDE) methods for cracked concrete and inspections to better quantify the extent of L Basin cracking and the potential regions of localized attack should be pursued. To facilitate this, untested, remaining C Core sample specimens that have rebar/concrete interfaces should be used to investigate rebar/concrete interactions in cracked concrete structures in conjunction with NDE techniques. Induced corrosion and NDE inspection could be correlated to create a benchmark for field inspections to supplement the structural integrity program (SIP). It is recommended that these remaining core segments be reserved for this type of pilot testing.

- Verification sampling and testing of the L Basin concrete to compare the microstructure, composition and profile of deleterious species to C Core sample results baseline.

TABLE OF CONTENTS

LIST OF TABLES

LIST OF FIGURES

LIST OF ABBREVIATIONS

amu	Atomic Mass Units
C-S-H	Calcium Silicate Hydrate
C3A	Tricalcium Aluminate
CLSM	Controlled Low Strength Material
DEF	Delayed Ettringite Formation
DSC	Differential Scanning Calorimetry
DTA	Differential Thermal Analysis
EDS	Energy Dispersive Spectroscopy
EXT	Exterior wall sample
IC	Ion Chromatography
ICP-ES	Inductively Coupled Plasma – Emission Spectroscopy
ISD	In Situ Decommissioning
ksi	kilo-pounds per square inch
NDE	Non-destructive Evaluation
NPH	Natural Phenomena Hazards
psi	pounds per square inch
RH	Relative Humidity
SEM	Scanning Electron Microscope
SIP	Structural Integrity Program
SRNL	Savannah River National Laboratory
SRS	Savannah River Site
TGA	Thermal Gravimetric Analysis
w/c	water to cement ratio
XRD	X-Ray Diffraction

1.0 Introduction

The L Area SIP[1] includes activities to support the on-going demonstration of the structural integrity of the L Basin. This program includes periodic inspection of the L Basin using underwater visual examination of the inside surfaces, and visual examination of below grade surfaces.

An assessment of the life expectancy of L Basin was published in 2008.[2] That assessment was based primarily on expert judgment of the physical properties and conditions of the basin materials. The conclusion of that assessment was the basin structures should perform the required functions against defined Natural Phenomena Hazards (NPH) events for an additional fifty years of service (through 2058), if maintained and protected from degradation. The L Area Structural Integrity Program had previously considered the harvesting and evaluation of concrete core samples to determine the extent of concrete degradation.[3] However, to negate the inevitable impact on operations, the viability assessment of life expectancy was performed instead of harvesting L basin concrete. Based on engineering judgment outlined in the assessment, the basin structures were expected to perform their required functions through 2020 (i.e., the anticipated end of service life in 2019).

By 2011, the uncertainty in duration for fuel storage in L Basin began to emerge and the basin end of service date sliding beyond 2020 had to be considered. Extended storage of fuel in L basin was critically evaluated in a topical report for extended fuel storage.[4] An augmented basin surveillance program was initiated which recommended activities such as core sampling and a materials degradation evaluation to strengthen the technical basis for basin integrity and life estimation. A plan was proposed for these activities in 2011[5] which describes tasks to sample concrete from facilities at SRS that contain concrete in a service-experienced condition representative of the L Basin, to avoid the impact on spent fuel project operations.

The location most representative of L basin was determined to be C basin due to its similar mission, service history, water chemistry standards and age. L basin de-ionizers came on-line in the 1990's and resulted in water chemistries with low conductivities, pH between 5.5 and 8 and chloride levels <1 ppm. This led to some difference in the service environment of the two basins such as C basin had higher water conductivity, chloride levels >10 ppm and pH between 8 and 9 during this interval of time. However, despite these differences, C basin was selected based on technical judgment of the L basin structural integrity team and SRNL with consideration given to concurrent operations in the facility. At this same time, C basin was being filled with Consolidated Low Strength Material (CLSM) as part of the In Situ Decommissioning (ISD) activities and action was required during FY12, prior to its closure date. Time constraints placed on the task required coring to not impact the ISD project schedule, funding and operational considerations increased the task complexity. An interior wall in the Monitor Basin was selected and core sampling was conducted as described in the technical report.[6] The cores were sectioned into segments for ease in shipping and are described in Figure 1. The segments were prepared for transport and shipped to SRNL for interim storage.

A technical path forward for the characterization of the concrete segments was drafted and proposed in 2013.[7] This approach focused on two aspects:

- Surveying the microstructure and chemistry of the concrete near the surface (i.e., 6 inch "A" segments), to determine any impact of basin water exposure on its condition and
- Characterizing the structural condition of the concrete by measuring its compressive strength in regions of uniform condition (i.e., 12 inch "C" segments).

In order to relate the two segments to one another, the materials in both segments were examined using a variety of characterization techniques. This report summarizes the test results analyzed to date.

The application of these results to trends in L basin relies on the premise that both L and C basins were constructed to equivalent design parameters, have had similar service histories and are of similar age. As mentioned before, the design drawings for both L and C basins call for 2500 psi concrete and 40 ksi reinforcing steel to be used. In addition, the materials were specified by the same Dupont Specification[8]. The design criteria for L and C basin structures are equivalent. The service histories of L and C basin have minor differences which primarily involve the use of frequent deionization as a result of upgrades in 1993.

This study focused on testing and analysis to quantify aging effects on the bulk concrete and the water contact region. The work did not explicitly address the following additional features of the concrete basin structure and the potential degradation phenomena that can cause weakness in the basin structure:

- Carbonation of above grade concrete (see reference 13)
- Degradation of exterior surface of concrete structure below grade from ground water
- Degradation of the waterstops
- Degradation of local regions including rebar/concrete interfaces associated with active leak sites

An outline of general activities is provided to evaluate these features and phenomena for potential impact to the long-term integrity of the L basin structure to perform its function for an extended storage mission.

2.0 Background

Both C and L Reactor buildings were constructed in the early 1950's to then Dupont Specification 3019, which is broad in scope[8]. The structural analysis calls for a minimum 2500 psi concrete and reinforcing steel which had a 40 ksi yield strength. Table 1 shows the codes and standards that specified the control of materials for the structure from Specification 3019. The engineering specification prescribed a minimum cement content for different classes of compression strength. For example, Class D or 2500 psi concrete specified a minimum of 4.4 cubic-feet (or ~430 lbs) cement per cubic yard of concrete. Cement was generally Type I (normal) or II (moderate sulfate resistance) Portland cement (with allowances for use of Type III for circumstances where high early strength was required). Fly ash was allowed (typically up to 15 % of cement by weight) and a composition was specified consistent with class F. Aggregate was typically quartz sand for fine aggregate (0.187 inch > diameter > 0.059 inch) and granite for coarse aggregate of diameter up to 1.5 inches (sometimes larger). Admixtures were also allowed for certain applications and air-entraining was also permitted in the range of 3 to 6%. Actual proportions of concrete materials were determined to meet performance requirements in the field (i.e., slump tests). Slump behavior of not more than 3 inches was specified in 3019 for mass placement but the actual slump was

dependent on the placement and could be as high as 6 inches. Maximum water to cement ratio (w/c) was specified by the testing laboratory and was prescribed to yield concrete of desired slump and placement characteristics. The w/c ratio typically ranged between 0.45 and 0.55.

In 1996, the Army Corps of Engineers analyzed concrete core and steel rebar samples from F- and H-Canyons at SRS which were built to the same specification as L area. The tests confirmed the design specifications and indicated that although no alkali-silica reaction was occurring, minor carbonation of the concrete was present.[9] Studies on saltstone vaults on-site have listed sulfate attack as the primary degradation mechanism for these concrete structures[10] due to the high concentration of sulfate and aluminate in the waste. Other studies also noted potential degradation mechanisms for above grade and below grade concrete[11] in a long term performance assessment of P reactor. The primary mechanism for the breakdown of the concrete below grade over time was concluded to be sulfate and magnesium attack. For above grade concrete, the controlling degradation mechanism is vegetative growth (if allowed) or carbonation and eventual corrosion of the steel reinforcement. Walton *et al.* [12] modeled the performance and degradation of concrete barriers for low level waste and quantified rates of concrete degradation for below grade structures. However, the degradation rates indicated in all these studies were extremely low. Above grade concrete was core sampled from areas in P and R reactor buildings[13]. No degradation in strength was observed (breaking strengths > 4000 psi) but more extensive carbonation was noted than in F and H canyons[9].

Based on the reports[10-12] which observed or predicted degradation mechanisms, C basin concrete was chosen to examine the potential for and extent of concrete degradation in L basin.

Table 1: Engineering Specification and Codes and Standards that controlled construction of Reactor Buildings at SRS.

Material	**Dupont Specification**	**National Standard**
Portland Cement	SB-1-A	ASTM C 150
Aggregate	SB-2-A, 3-A	ASTM C 33
Water	SB-5-A, 6-A	AASHTO T26
Reinforcement	SB 4-A	ASTM A 15, A305
Fly Ash	3019	
Testing	SB-5-A	
Proportioning/Batching/Mixing	SB-6-A	
Placement	SB-8-A, 9-A	
Finishing	SB-10-A	
Curing	SB-11-A	

2.1 Degradation Mechanisms

Potential degradation mechanisms that occur in concrete can be chemical (leaching/dissolution) and mechanical (e.g., cracking) in nature. Although many of these were not observed in the samples analyzed, these are the typical mechanisms seen to reduce the strength and integrity of concrete structures. They are briefly summarized here for reference.

Sulfate attack occurs as a result of sulfur in pore water reacting with a phase in the concrete (tricalcium aluminate or C3A) to form hydrated calcium aluminum sulfates (i.e. ettringite). Similarly, Carey[11] noted the reaction of magnesium in pore water with the cement to form Brucite ($Mg[OH]_2$). The formation of these phases results in expansion and can lead to cracking and disintegration of the cementitious structure. If sulfates originate from groundwater intrusion, the degradation occurs along a moving front. If sulfates leach from aggregates or the cement itself, the degradation is more generalized and occurs throughout the structure. The ASTM C 150 standard, specification 3019, limits sulfur content to minimize the extent of this degradation.

Corrosion of steel rebar is accompanied by a 3-6X volumetric expansion due to the corrosion products, which leads to severe cracking and degradation of the concrete cover, usually associated with spalled concrete fragments. General corrosion (or pitting corrosion) is more commonly seen and can result from two mechanisms: carbonation of calcium rich phases and halide (e.g., chloride) induced corrosion. Furthermore, the corrosion itself can be divided into two phases: initiation and corrosion phases.

Chloride ingress can cause localized de-stabilization of the passive film of iron oxide that would be present on reinforcement bars embedded in the concrete (i.e., initiation), and lead to pitting corrosion. If carbonation reaches the depth of the reinforcement bars, the passive film breakdown would be widespread and general rebar corrosion would be expected, leading to spallation. In short, chloride ingress alone would cause localized (i.e., pitting) attack, but along with carbonation, more general steel corrosion would occur.

Carbonation of concrete allows passive film breakdown by reducing the local pH of the pore water due to the reduced solubility of calcium carbonate when compared to calcium hydroxide in water. It occurs as a result of diffusion of carbon dioxide and the conversion of portlandite ($Ca[OH]_2$ or calcium hydroxide) to calcium carbonate or calcite ($CaCO_3$). Many factors can affect the rate of carbonation, including temperature, relative humidity, and composition of the cement paste.

Alkali-Silica reactions (ASR) occur between reactive silica present in aggregates and alkali constituents (e.g., Na+, K+) in the cement phase(s). In similar fashion to sulfate attack, the alkali constituents form a gel at the aggregate/cement interface, which causes expansion and cracking to occur over time. Water, reactive silica and alkali constituents must be present in the concrete for ASR to occur. Reactive silica (e.g., opal, chert or chalcedony) can exist in aggregates of volcanic origin and are less common in igneous rock. The crystallographic structure may be identical, but the crystal size is much smaller in the case of reactive silica. Sand (a common fine aggregate) is also quartz, but is usually not reactive because it is the residual component following mechanical and chemical degradation of rock. Specification 3019 limits the use of reactive aggregate content to prevent this type of degradation. In order to verify the occurrence

of ASR, petrography or scanning electron microscopy (SEM) with energy dispersive spectroscopy (EDS) must be performed on samples to identify the gel reaction zones.

As concrete is exposed to water, cement compounds will be leached from the concrete. Initially, alkali metal hydroxides (NaOH, KOH and LiOH) are leached from the cement. Then, calcium hydroxide ($Ca[OH]_2$) begins to be depleted. Once $Ca[OH]_2$ becomes depleted, the hydrated cement phases begin to dissolve. The leaching of calcium hydroxide tends to lower the strength of the concrete and induce other degradation mechanisms, such as rebar corrosion.

Other phenomena that lead to degradation of concrete structures include: microbial induced corrosion, freeze thaw, vegetative growth and cracking. The characterizations of these are difficult to conduct and were not considered in this analysis. However, the concrete structures at SRS are not immune from these phenomena and any thorough prediction of service life should bear them in mind.

3.0 Methods

The scope of work for this testing program is documented in a previous report[7]. A total of five core sections were removed from C basin. Each section was approximately 4 feet in length and 6 inches in diameter. All five cores were visually observed to be free of cracks, flaws and other gross defects as removed. The cores were marked and labeled prior to sectioning with the number corresponding to its position and the letter corresponding to the proximity from the surface of the wall (e.g., 1A: at surface, 1B: beneath surface, etc.).

In Figure 1, a schematic demonstrates the method by which the cores were sectioned and labeled. Although the concrete appears to be in good condition, absolute identification of potential degradation mechanisms can only be accomplished through a detailed laboratory analysis of samples obtained from the structure. The laboratory analysis focused on: 1) materials characterization of the near surface segments to identify any reactions with the service environment and 2) a quantitative measure of degradation due to loss in mechanical strength in the internal segments. In order to perform this analysis, a deliberate, disciplined testing scheme was employed. The results of tests performed on core samples will provide the basis for a degradation model in support of structural integrity.

3.1 Materials Characterization

The samples were analyzed using a number of different techniques. To enable phase identification, X-ray Diffraction (XRD) was utilized on pulverized concrete samples. In order to adequately characterize the microstructure, optical microscopy and SEM/EDS were conducted on cross-sectioned portions of the concrete. Chemical content was measured using inductively coupled plasma – emission spectroscopy (ICP-ES) on dissolved solutions from pulverized samples. Carbon (C) and sulfur (S) content were determined by performing Leco C/S analysis on pulverized samples. The extent of carbonation was visually checked during sectioning. The water content and other volatile species were determined by Thermal Gravimetric Analysis (TGA).

3.1.1 Sectioning

Initially, the characterization of the concrete involved sectioning the near surface segment (labeled "A") of three cores. The painted surface was determined to be a polychlorinated biphenyl (PCB) hazard so the painted surface and 0.5 in. of concrete beneath it were removed by sectioning the "A" segment parallel to the water exposed surface. This was conducted on a Buehler Delta Orbital Cutter with a water cooled 16 in. diamond impregnated sectioning blade. The painted section was disposed of as hazardous waste. After this, the "A" segment was sectioned along the cylinder and radial axes to produce a cylinder sector. This sector was then sliced at regular intervals parallel to the original surface in order to isolate material from a uniform distance beneath it (see Figure 1). The first sample was taken 0.5 in. from the water exposed surface. The second through seventh samples were sectioned at 0.25 in. increments. The eighth, ninth and tenth samples were sectioned at 0.5 in. increments, while samples eleven and twelve were sectioned at 1 in. increments up to 5.5 in. beneath the surface. A full list of samples sectioned from each core is contained in Table 2 along with the analysis techniques.

3.1.2 Depth of Carbonation

An acid-base indicator solution of 1% phenolphthalein solution was applied to a newly exposed cross-sectioned surface of each core.[14] If the sample is unaffected by carbonation, the solution turns pink; if there is carbonation present, the concrete does not change color. The pH and chemical composition of the concrete can be estimated based on the color of the solution after it has been applied to the concrete. These results will be used to estimate the rate of carbonation of the reactor building walls and therefore the susceptibility to degradation through corrosion of the steel reinforcement.

3.1.3 Microstructural Analysis

The microstructure of the concrete was inspected visually, sectioned, mounted and polished down successively down to 1 micron diameter diamond abrasives. Areas of interest were identified using optical microscopy. The samples were carbon coated and analyzed using SEM/EDS. Micrographs of the core samples were taken using SEM to determine the microstructure of the concrete and EDS was used to determine the distribution of phases such as ettringite, portlandite, and calcium silicate hydrates (C-S-H) throughout the sample. The character of the aggregates was also examined.

Select samples were pulverized to a fine powder and analyzed using X-ray powder diffraction (XRD). The randomized crystals of the sample were then subjected to a collimated beam of monochromatic X-rays which interact with the sample to produce constructive interference and diffracted rays at characteristic incident angles. The governing principle that defines the relationship between the X-ray beam and the diffracted rays is known as Bragg's Law ($n\lambda=2d \sin\theta$). This law relates the wavelength of electromagnetic radiation to the diffraction angle and the atomic lattice spacing in a crystalline sample. The diffracted X-rays are counted and by scanning the sample through a range of 2θ angles, all possible diffraction directions of the lattice(s) should be attained due to the random orientation of the powder. Each mineral phase has a unique set of peaks which correspond to lattice spacing (i.e., d-spacings) Identification of mineral phases is typically achieved by comparison of d-spacings with standard reference patterns. For mixed materials, detection limit of this technique is ~ 2% of sample.

3.1.4 *Chemical analysis*

Pieces of the cores near the surface were taken as a function of depth and pulverized into a fine powder for chemical analysis. A portion of the powder from each sample underwent a cesium carbonate (Cs_2CO_3) fusion at 950 ºC to breakdown the structure. It was then dissolved in diluted sulfuric acid for analysis. The concentrations of cations were determined using ICP-ES. Anions in solution were determined using ion chromatography (IC). The overall composition was estimated by assuming the most stable compound stoichiometry for each oxide.

A portion of pulverized samples were analyzed using a Leco CS 230 carbon/sulfur determinator that is contained in a radiological glovebox. The samples were run in accordance with SRNL reference procedure L29-ITS-0201.[15] Samples were analyzed in duplicate with 0.5 g sample size per analysis. The results were reported in μg/g on an elemental basis and converted to CO_2 and SO_4 basis in weight percent.

Selected samples from core sections were also analyzed using thermogravimetric analysis (TGA) coupled with a mass spectrometer to determine the content of volatile species (water, carbon dioxide and sulfate). Measurements were made using a Netzsch STA 409 PC Luxx® thermogravimetric analyzer (TGA) and a Pfeiffer Thermostar™ mass spectrometer (MS). A high-purity (99.995%) argon purge stream passes through the TGA sample chamber, then to a sample point where the MS continuously samples the TGA off-gas. The TGA-MS is calibrated for moisture using gypsum ($CaSO_4 \cdot 2H_2O$) standards.

3.2 Compression Tests

Compression testing was utilized to determine the compressive breaking strength of the concrete structure. This information was used to demonstrate the validity of the design parameters of the structure. The interior portions (labeled “C” segments) of the concrete cores were used for compression tests. The diameter of each core was 5.6 inches X 11.3 inches in order to minimize any effect of aggregate on breaking strength. Prior to the test, the cylinders were measured to confirm the dimensions were in accordance with ASTM C 42[16]. End caps (with compression pads) were place on each end of the test cylinder to ensure that the test load is uniformly distributed for consistent breaks. Then the samples were double wrapped in plastic to contain the sample debris upon fracture and to limit the spread of contamination. The testing was performed in accordance with ASTM C 1231[17] on a Humboldt HCM-0030 Series load frame with a capacity of 300,000 lbs. The cylinder/end caps/plastic bag assemblies were tested to failure at a loading rate of 35 ± 7 psi/s. After the test, the bag was surveyed for contamination and the assembly was transferred to a bench and disassembled to examine the fractured concrete for the presence of defects or unusual features that would have resulted in premature fracture. The load was used to calculate the compressive stress at failure.

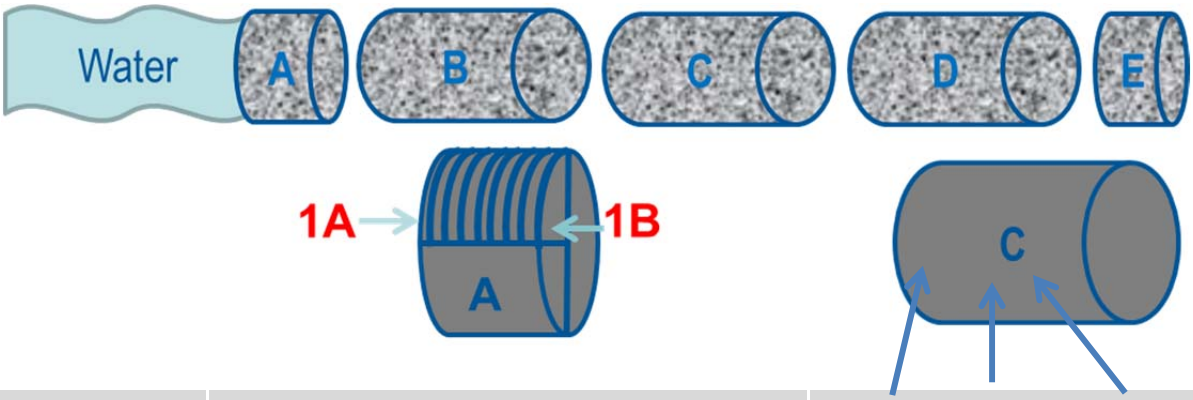

Core Segment	A	C
Sample # methodology	# A – # A or B - # # Core # and Segment Letter # and Letter within Segment # relative depth from surface	# C – **top, mid and bot** Core # and Segment Letter relative position from inside core

Figure 1: Sample characterization scope and explanation of labeling sequence for samples with respect to position in the core

Table 2: Sample Characterization Scope of Program

Sample Number	Distance from water surface (inches)	Elevation from below grade (inches)	Optical Micros-copy.	SEM	EDS	XRD	Dis-soltn ICP	Leco C/S	TGA Mass Spec.
1A-1A-1	0.5	66	-	-	-	-	X	X	-
1A-1A-2	0.75	66	X	X	X	-	-	-	-
1A-1A-3	1.0	66	-	-	-	-	X	X	-
1A-1A-4	1.25	66	-	-	-	-	-	-	-
1A-1A-5	1.5	66	-	-	-	-	X	X	-
1A-1A-6	1.75	66	X	X	X	-	-	-	-
1A-1A-7	2	66	-	-	-	X	X	X	-
1A-1B-8	2.5	66	-	-	-	-	X	X	-
1A-1B-9	3	66	-	-	-	-	-	-	-
1A-1B-10	3.5	66	-	-	-	-	X	X	-
1A-1B-11	4.5	66	X	X	X	-	-	-	-
1A-1B-12	5.5	66	-	-	-	-	X	X	-
1C-top	> 18	66	X	X	X	-	-	-	-
1C-mid	> 18	66	X	X	X	-	-	-	-
1C-bot	> 18	66	-	-	-	-	-	-	-
4A-1A-1	0.5	66.5	X	X	X	-	X	X	-
4A-1A-2	0.75	66.5	X	X	X	-	-	-	-
4A-1A-3	1.0	66.5	-	-	-	-	X	X	-
4A-1A-4	1.25	66.5	-	-	-	-	-	-	-
4A-1A-5	1.5	66.5	-	-	-	-	X	X	-
4A-1A-6	1.75	66.5	X	X	X	-	-	-	-
4A-1A-7	2	66.5	-	-	-	X	X	X	-

Table 2: Sample Characterization Scope of Program (cont.)

Sample Number	Distance from water surface (inches)	Elevation from below grade (inches)	Optical Micros-copy	SEM	EDS	XRD	Dis-soltn ICP	Leco C/S	TGA Mass Spec.
4A-1B-8	2.5	66.5	-	-	-	-	X	X	-
4A-1B-9	3	66.5	-	-	-	-			-
4A-1B-10	3.5	66.5	-	-	-	-	X	X	-
4A-1B-11	4.5	66.5	X	X	X	-	-	-	-
4A-1B-12	5.5	66.5	-	-	-	-	X	X	-
4C-top	> 18	66.5	X	X	X	-	-	-	-
4C-mid	> 18	66.5	X	X	X	-	-	-	-
4C-bot	> 18	66.5	X	X	X	-	-	-	-
5A-1A-1	0.5	72	-	-	-	-	X	X	-
5A-1A-2	0.75	72	X	X	X	-	-	-	-
5A-1A-3	1.0	72	-	-	-	-	X	X	X
5A-1A-4	1.25	72	-	-	-	-	-	-	-
5A-1A-5	1.5	72	-	-	-	-	X	X	-
5A-1A-6	1.75	72	X	X	X	-	-	-	-
5A-1A-7	2	72	-	-	-	X	X	X	X
5A-1B-8	2.5	72	-	-	-	-	X	X	-
5A-1B-9	3	72	-	-	-	-	-	-	-
5A-1B-10	3.5	72	-	-	-	-	X	X	-
5A-1B-11	4.5	72	X	X	X	-	-	-	-
5A-1B-12	5.5	72	-	-	-	-	X	X	X
5C-top	> 18	72	X	X	X	-	-	-	-
5C-mid	> 18	72	X	X	X	-	-	-	-
5C-bot	> 18	72	X	X	X	-	-	-	-

4.0 Results and Discussion

The analysis of the concrete cores is presented in this section. The results are organized into two categories. First, the microstructure and chemistry of the concrete in near surface segments has been studied. This was studied to determine any impact of basin water exposure on the condition of the concrete. Second, the structural condition of the concrete was studied by measuring its compressive strength in interior segments (i.e., 12 inch C segments). Also, the microstructural analysis of the concrete relates the "C segments" from inside the wall to the near surface segments.

4.1 Near Surface Core Segments

4.1.1 Depth of Carbonation

Carbonation is a primary cause of long-term degradation in concrete structures as a result of CO_2 diffusing from the surrounding medium which reduces the concrete pH from basic toward neutral.[12, 14]

Figure 2 shows sections from three core samples in C basin which have been tested for carbonation using the 1% phenolphthalein solution. Although the first 0.5 in. of the concrete sample was removed with the painted section, no carbonation is visible beneath this layer.

4.1.2 Phase Identification

X-ray diffraction (XRD) was conducted on select samples from C basin to observe which phases are present in the concrete. Figure 3 - Figure 5 show sample XRD results from sections of the three core segments from approximately 2 inches from the water surface. A summary of the phases observed is presented in Table 3. The presence of several aggregate phases is expected. Many phases prominent in granite (e.g., albite, microcline, muscovite and quartz) are observed to be present in all scans. Either portlandite ($Ca[OH]_2$) or calcite ($CaCO_3$) are noted in the samples which originate from the cement paste. Calcite is actually a reaction product of portlandite and carbon dioxide. Silica (SiO_2) is the prominent phase in all scans and is expected due to its concentration in aggregates and the cement paste. Ettringite was not identified by XRD analysis so it may not be present in significant quantity to be detected.

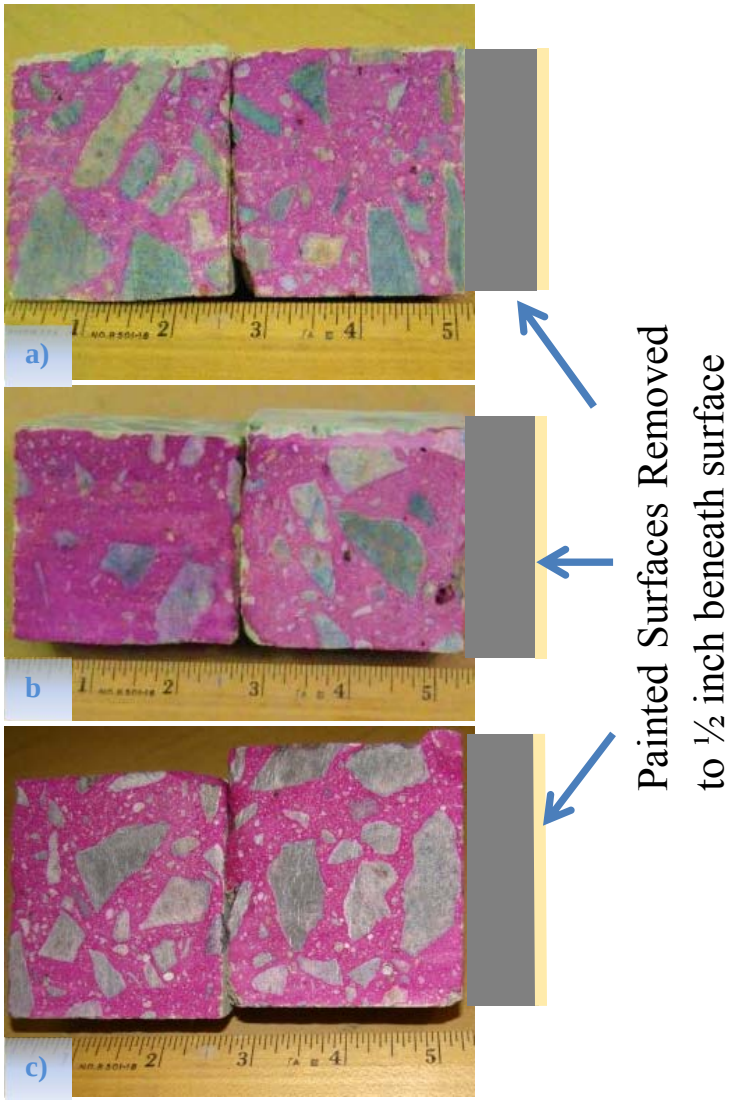

Figure 2: Cross section of A core segments 1 (a), 4 (b) and 5 (c) from near surface concrete of C basin wall sections; the pink color of the phenolphthalein indicator shows no carbonation saturation was observed.

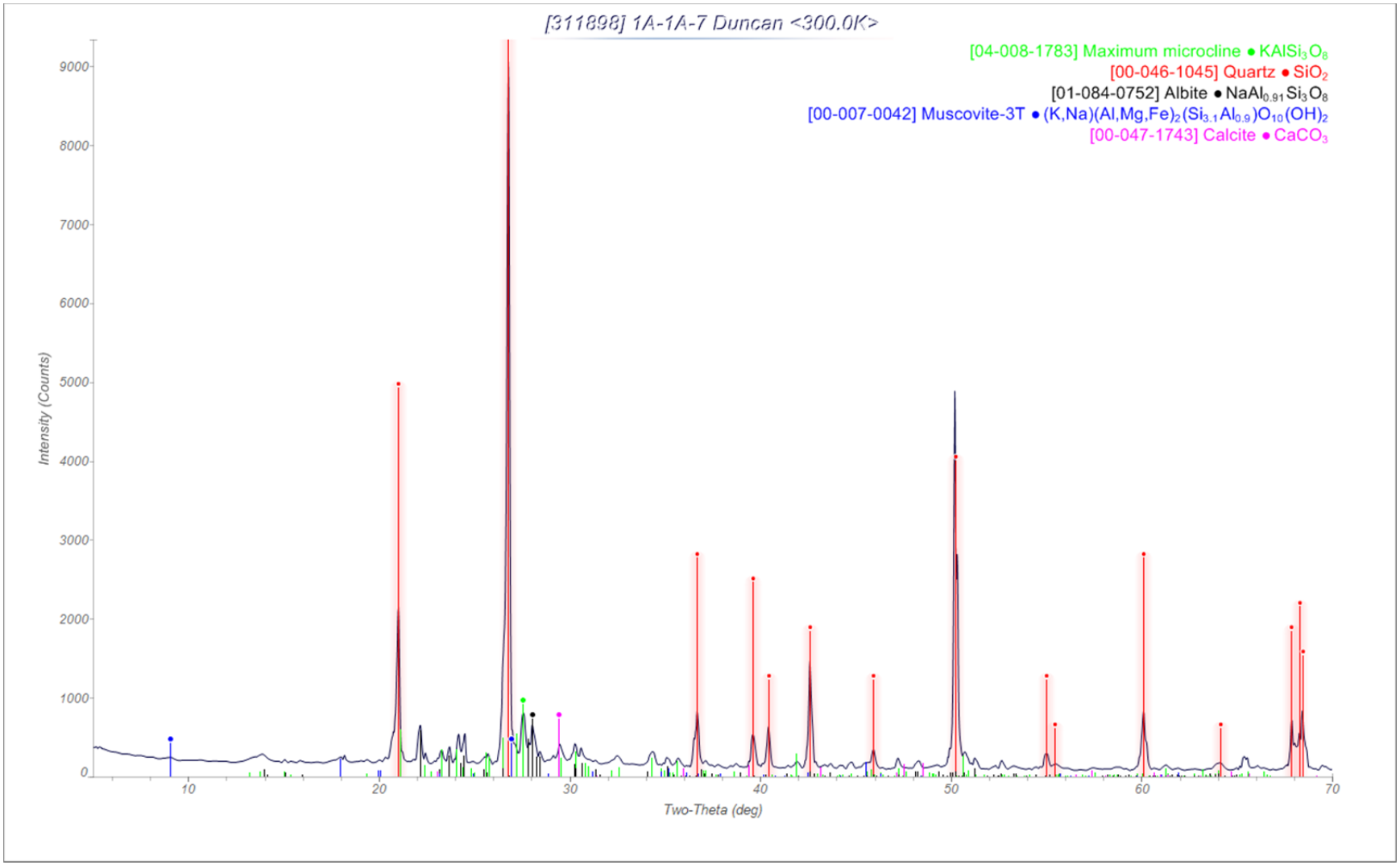

Figure 3: XRD scan of pulverized concrete from concrete sample 1A-1A-7

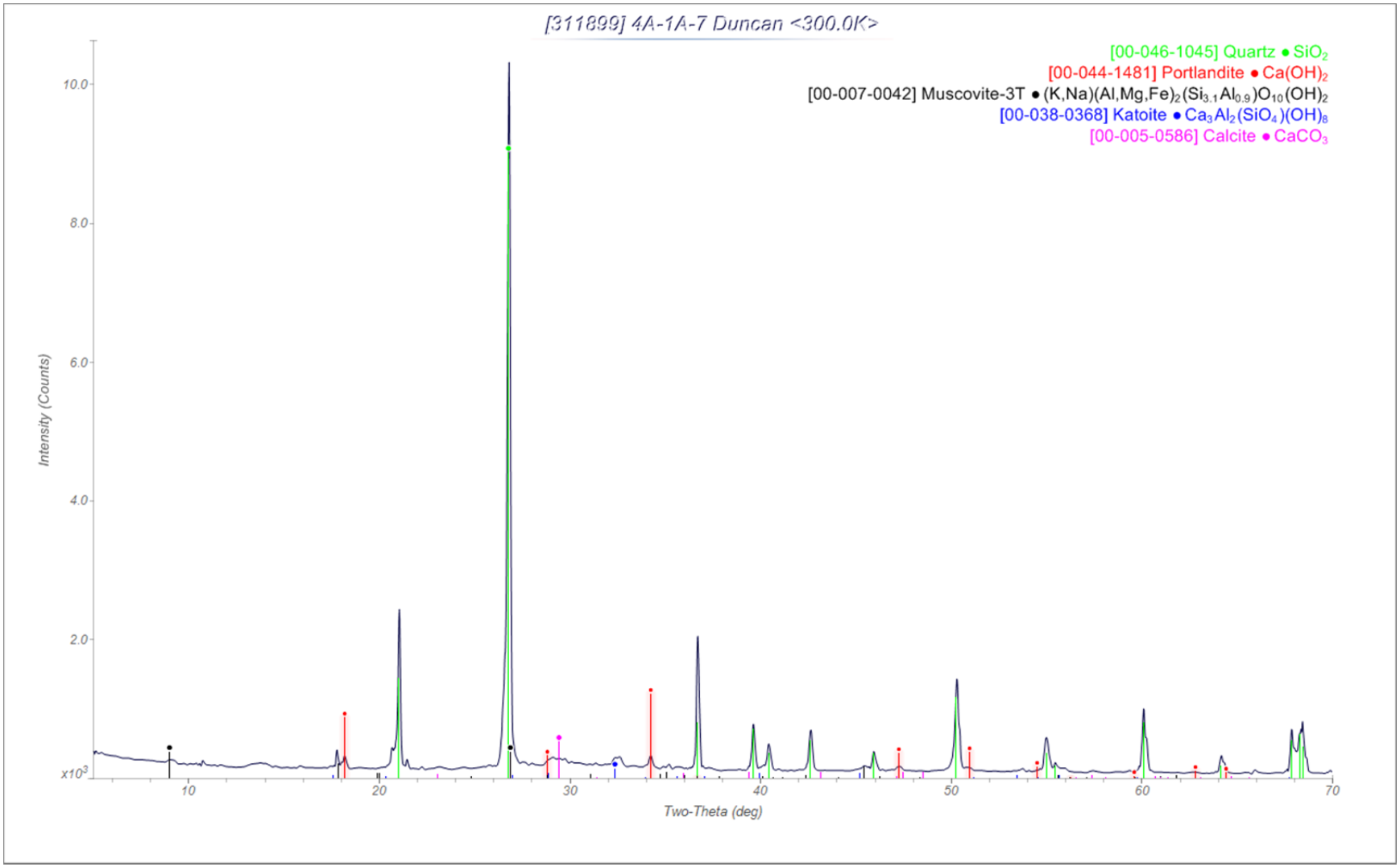

Figure 4: XRD scan of pulverized concrete from concrete sample 4A-1A-7

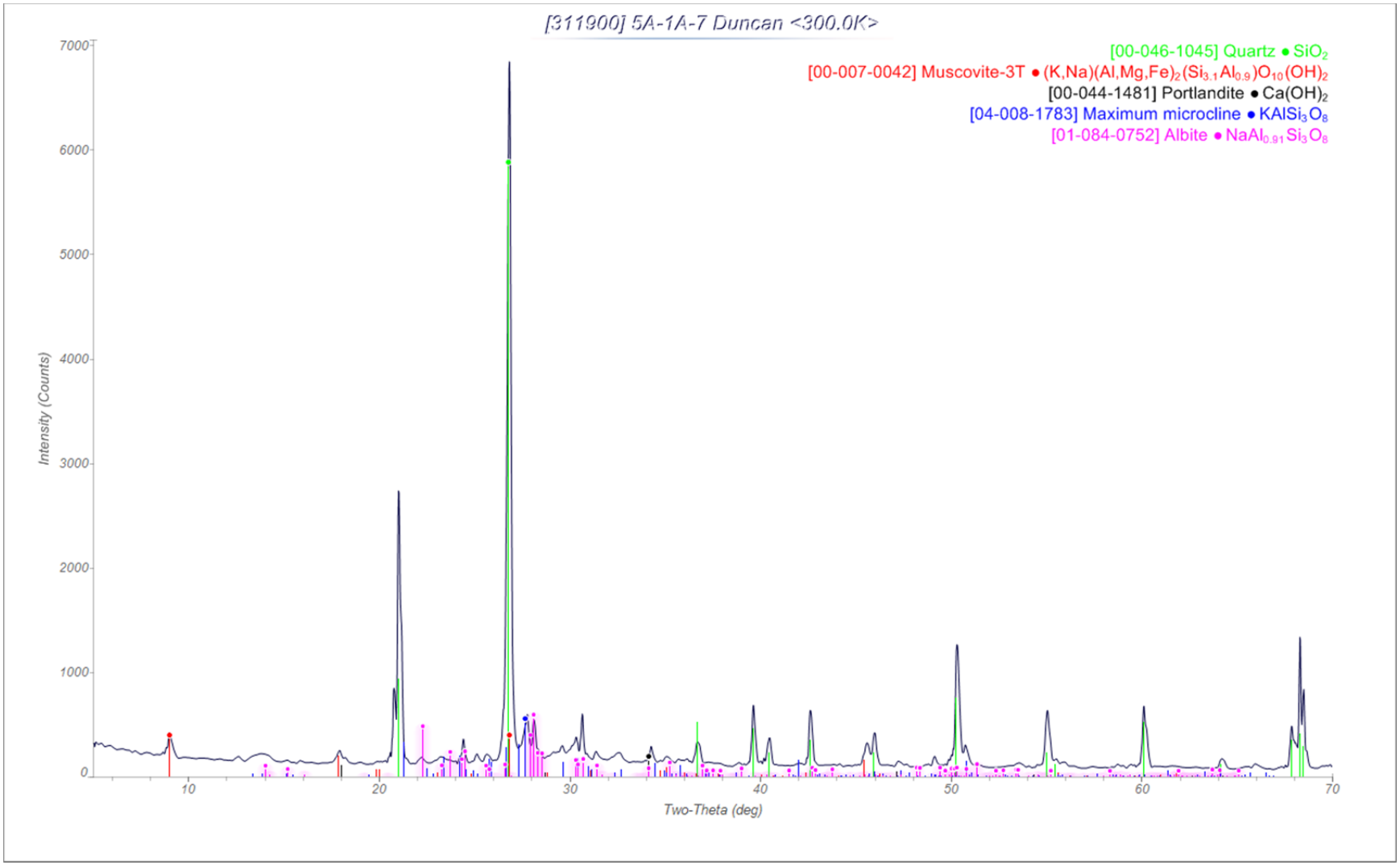

Figure 5: XRD scan of pulverized concrete from concrete sample 5A-1A-7

Table 3: Phases identified as prominent in samples from cores 1, 4 and 5 (2 inch depth) using X-ray diffraction along with their most likely source.

Phase	Present in Core	Cement	Aggregate	Impurity
Microcline-$KAlSi_3O_8$	1 and 5		X	
Quartz-SiO_2	1, 4 and 5	X	X	
Muskovite-3T	1, 4 and 5		X	
Albite-$NaAlSi_3O_8$	1 and 5		X	
Portlandite-$Ca(OH)_2$	4 and 5	X		
Katoite-$Ca_3Al_2(SiO_4)_{3-x}(OH)_{4x}$	4		X	
$CaCO_3$	1 and 4	X		X

4.1.3 SEM Microanalysis

The C basin concrete core samples were sectioned and polished for SEM/EDS analysis. The back scattered electron (BSE) micrographs representative of the microstructure in each sample are presented in Figure 6 through Figure 14. Phases are labeled where EDS data effectively identified the composition of phases present. Based on the elemental composition of the aggregates and cement paste phases, the presence of ettringite ($CaAl[SO4]_3[OH]_{12}\bullet 26H2O$) was noted throughout the samples. This whisker like phase precipitates from calcium, aluminum and sulfur contained in pore water and fills the void space present in concrete. It is not understood why ettringite is so apparent in the SEM samples yet not observed in the XRD results although SEM is more sensitive than XRD. Figures 8 through 12 show large air voids that have been filled to some extent with ettringite. This is expected to occur in the presence of moisture and is commonly observed in concrete.[18] The presence of microcracks (i.e., dark lines or areas) can be seen in several micrographs (particularly around ettringite formations). It is important to note, however, that the cracks did not appear to be undermining the stability of the concrete.

In addition to ettringite, several phases that are consistent with granitic formations were identified in the large aggregates phases (e.g., microcline, iron oxides, ilmenite and quartz). Quartz also made up the majority of fine aggregates but the presence of microcline ($KAlSi_3O_8$), Fe oxides, ilmenite ($FeTiO_3$) and zircon ($ZrSiO_4$) were also observed. This is consistent with aggregates used in structural concrete. Alkali-silica gel was not observed to be prevalent in the structure.

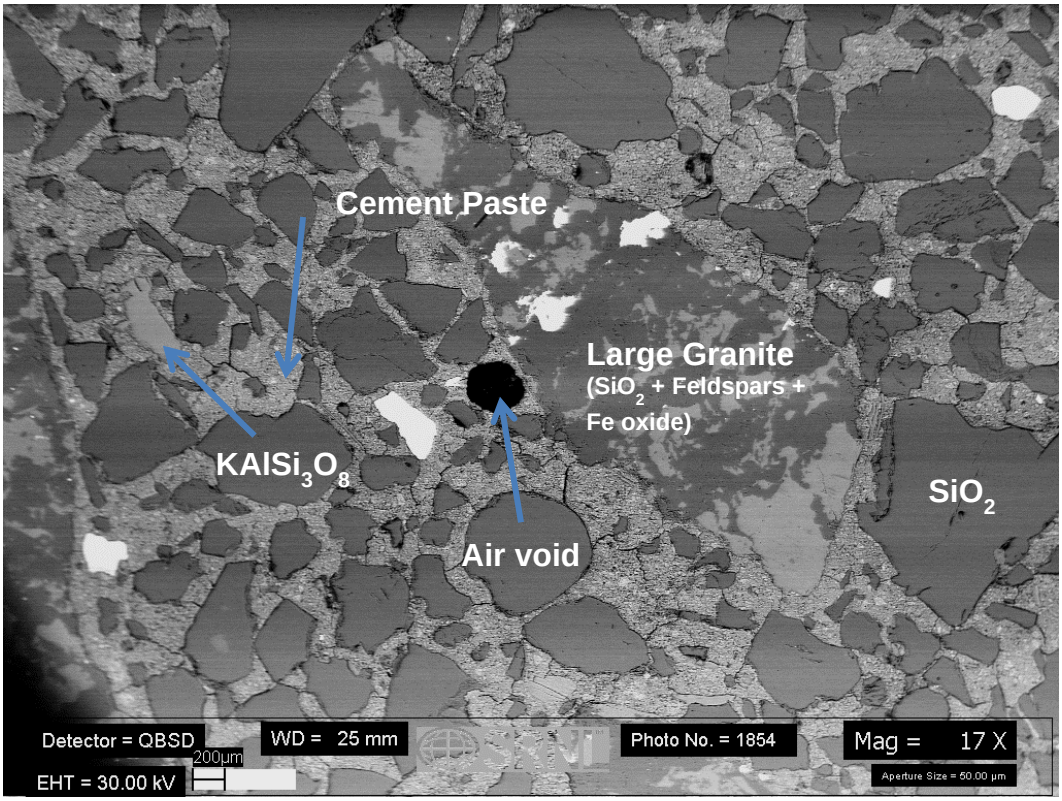

Figure 6: SEM backscattered electron photomicrograph of a cross-sectioned sample 1A-1A-2.

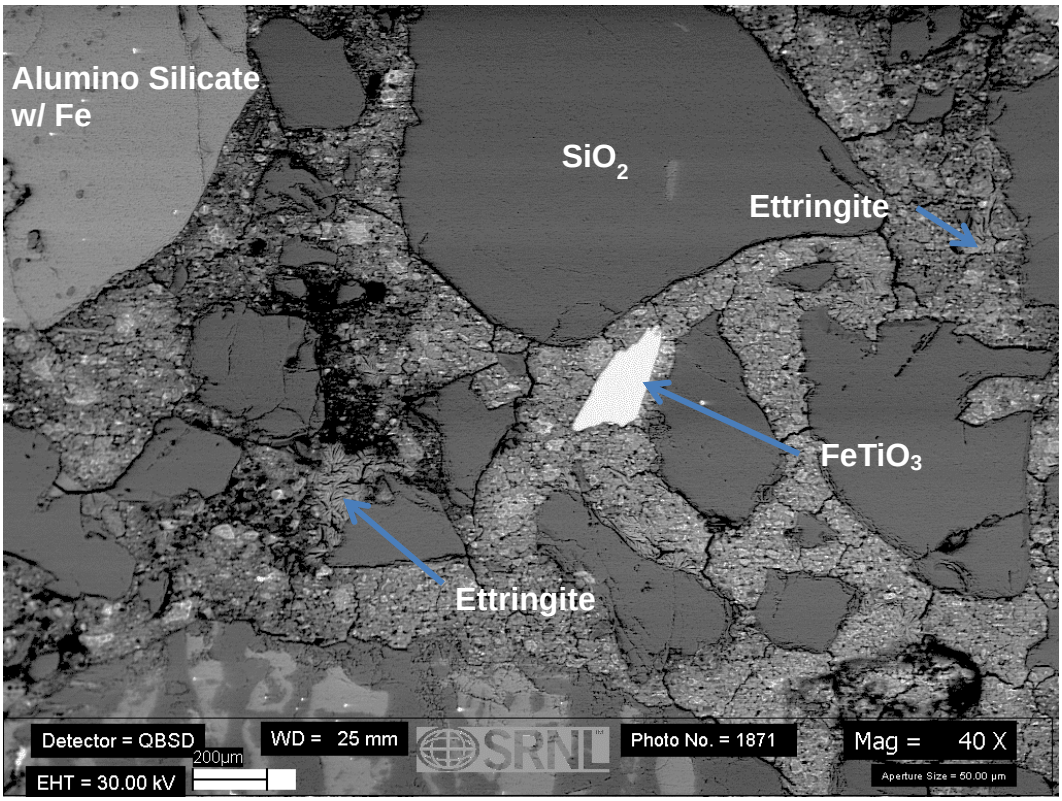

Figure 7: SEM backscattered electron photomicrograph of a cross-sectioned sample 1A-1A-6.

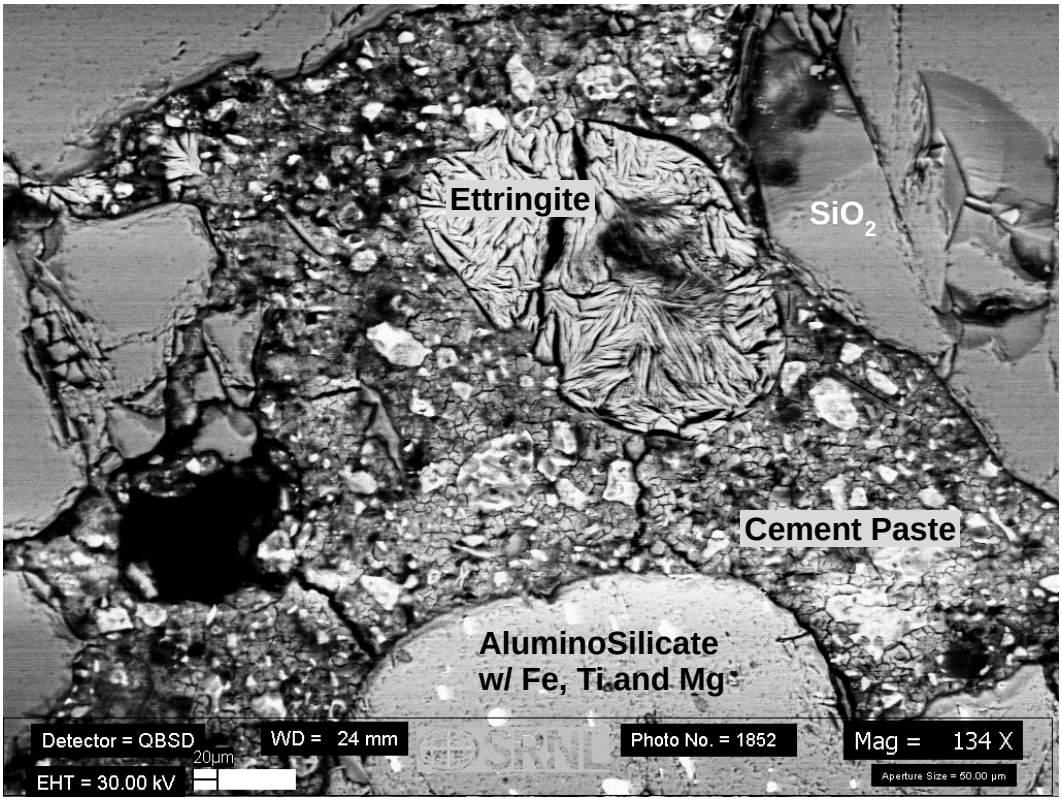

Figure 8: SEM backscattered electron photomicrograph of a cross-sectioned sample 1A-1B-11.

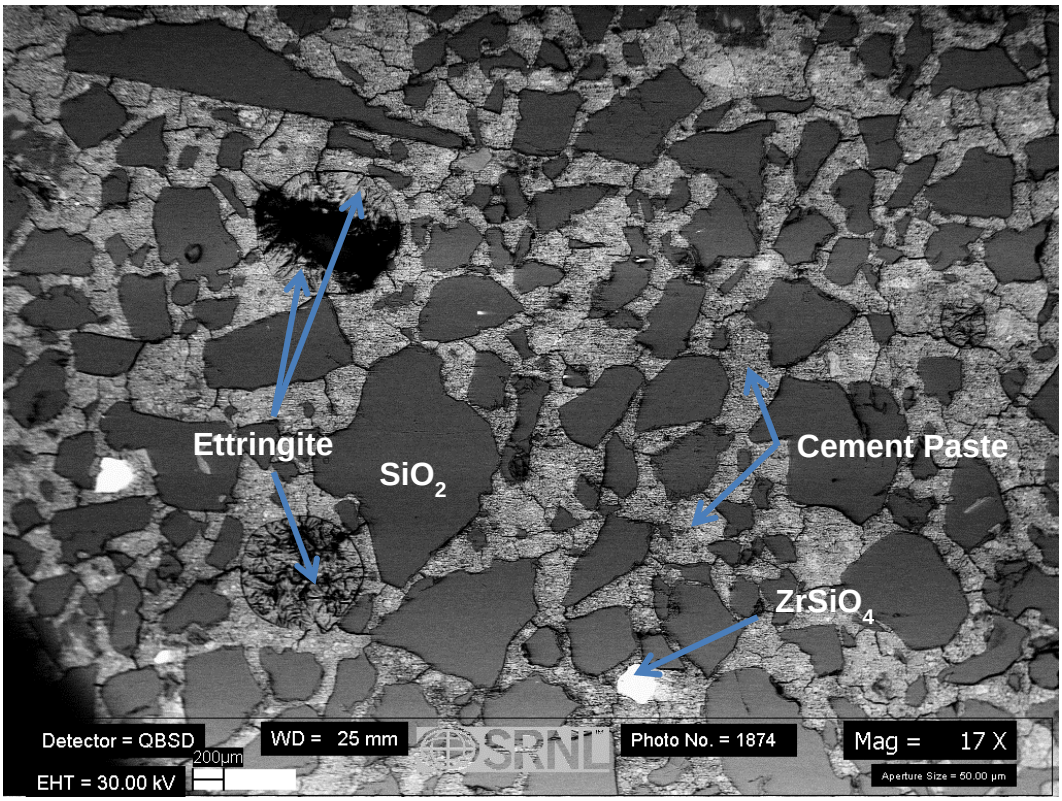

Figure 9: SEM backscattered electron photomicrograph of a cross-sectioned sample 4A-1A-2.

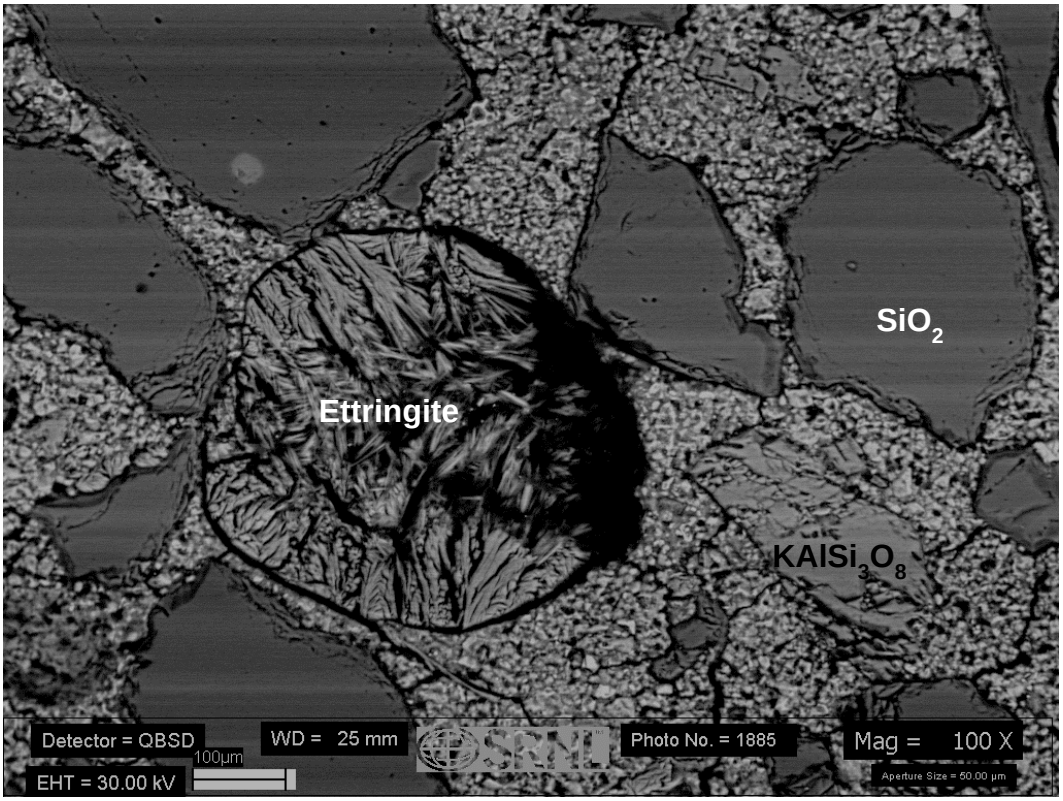

Figure 10: SEM backscattered electron photomicrograph of a cross-sectioned sample 4A-1A-6.

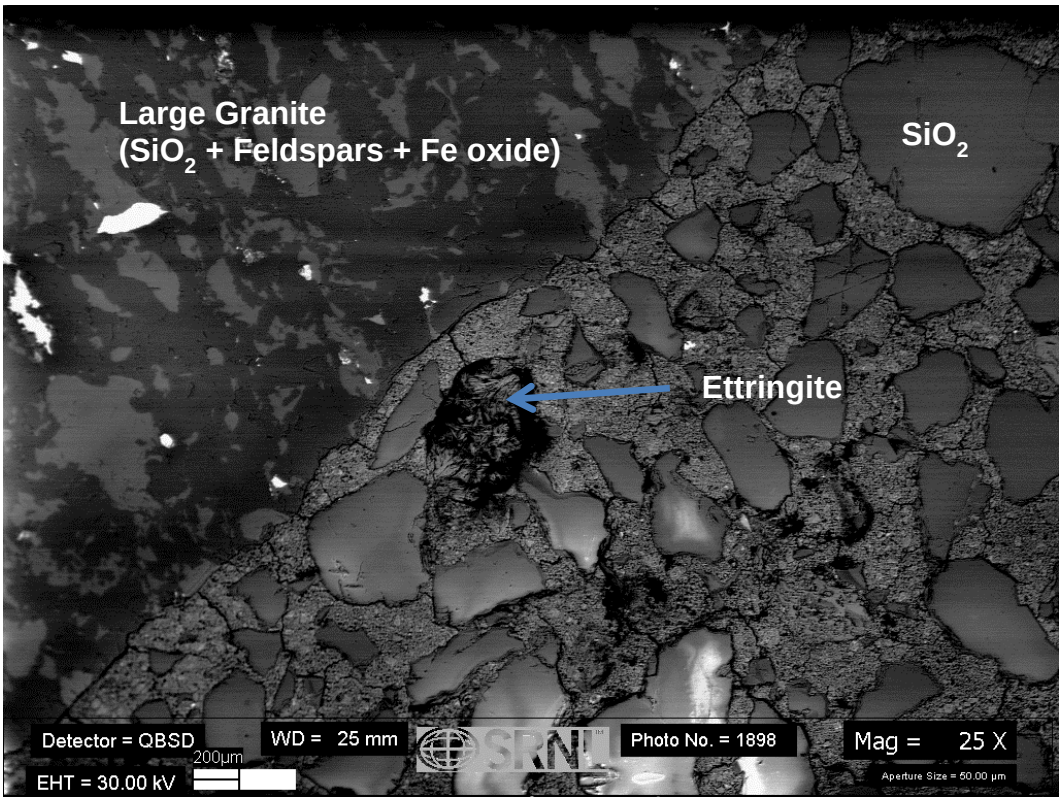

Figure 11: SEM backscattered electron photomicrograph of a cross-sectioned sample 4A-1A-6.

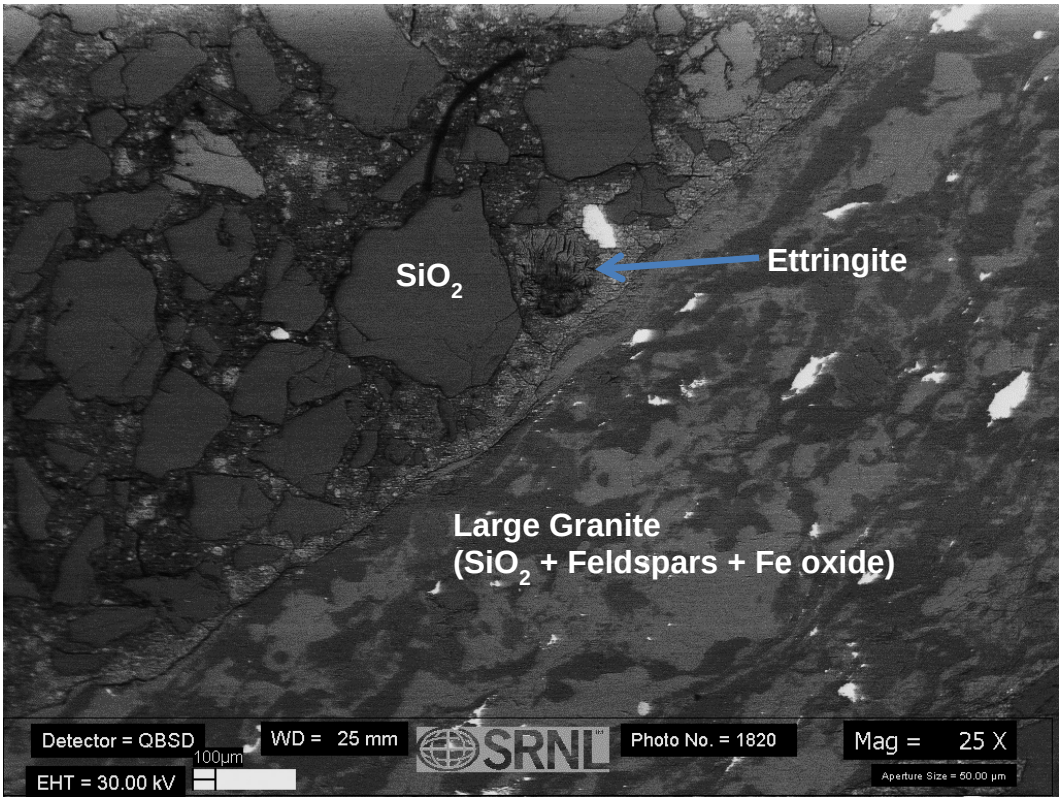

Figure 12: SEM backscattered electron photomicrograph of a cross-sectioned sample 5A-1A-2.

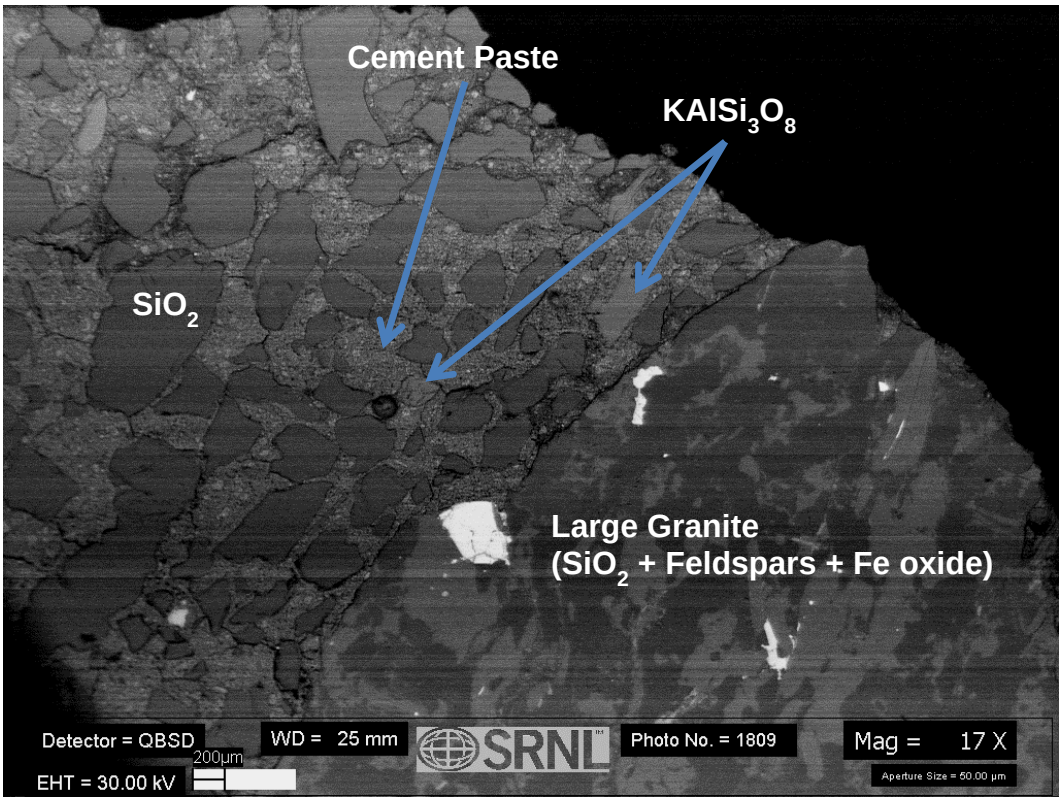

Figure 13: SEM backscattered electron photomicrograph of a cross-sectioned sample 5A-1A-6.

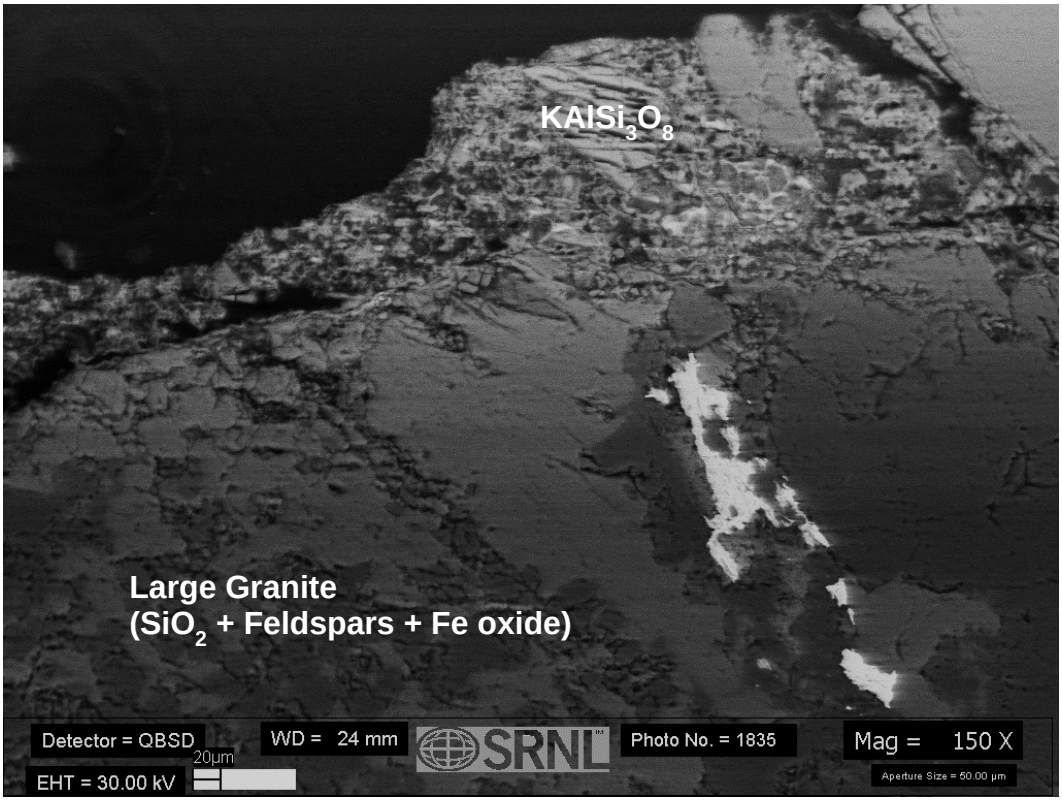

Figure 14: SEM backscattered electron photomicrograph of a cross-sectioned sample 5A-1B-11.

4.1.4 Chemical Analysis

The depth composition profiles of samples from each core were determined for a large number of elements. However, to simplify the analysis, the primary cations were considered. The concentration gradients of calcium, silicon and aluminum oxides are shown in Figure 15, Figure 16 and Figure 17 for Core 1, 4 and 5, respectively. If an extensive reaction between basin water and concrete has occurred, a concentration gradient should exist in the most soluble elements (i.e., Ca^{++}). As is evident from Figures 15-17, no significant concentration gradient for calcium oxide is present. Anion analysis to look for species such as chloride, fluoride, bromide, nitrite, nitrate, phosphate and oxalate was conducted and levels were all measured below the threshold of detection (<10 ppm in most cases). Significant levels of chloride and other deleterious species were not observed.

Sulfate could not be measured by IC due to the use of sulfuric acid in digestion. Hence, LECO carbon sulfur analyses were performed on the same samples as those presented in Figures 16 and 17 which were not subjected to the $CsCO_2$ fusion or dissolution in sulfuric acid. The sample results are presented in Figure 18 and 19. The horizontal lines on each graph represent the limits of CO_2[a] or sulfate ions expected in the samples based on the mix design estimates and the ASTM standard specification.[19] As can be seen

[a]The limits of CO_2 depend on the levels of calcium available in the matrix for reaction and vary with the microstructure and mix design. Previous studies[13] have observed 6% CO_2 is enough to saturate the concrete so 50% of this value was chosen as a point of reference.

in both figures, the sulfate concentration in the interior sample remains constant around 0.3 %. Levels of this magnitude would not be seen in the spectra for XRD. The CO_2 content in both samples is roughly 0.8% which is below a level expected to form a carbonation front.[13] Hence, significant levels of carbon dioxide or sulfur have not been observed.

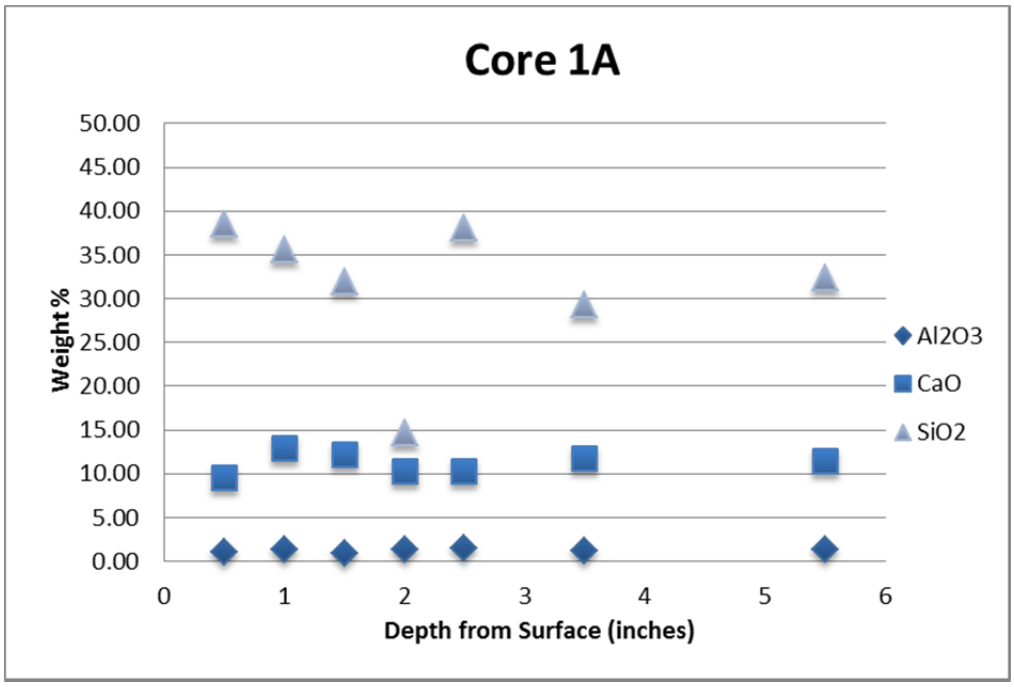

Figure 15: Concentration of Aluminum, Calcium and Silicon oxides as a function of depth beneath the surface for Core segment 1A.[a]

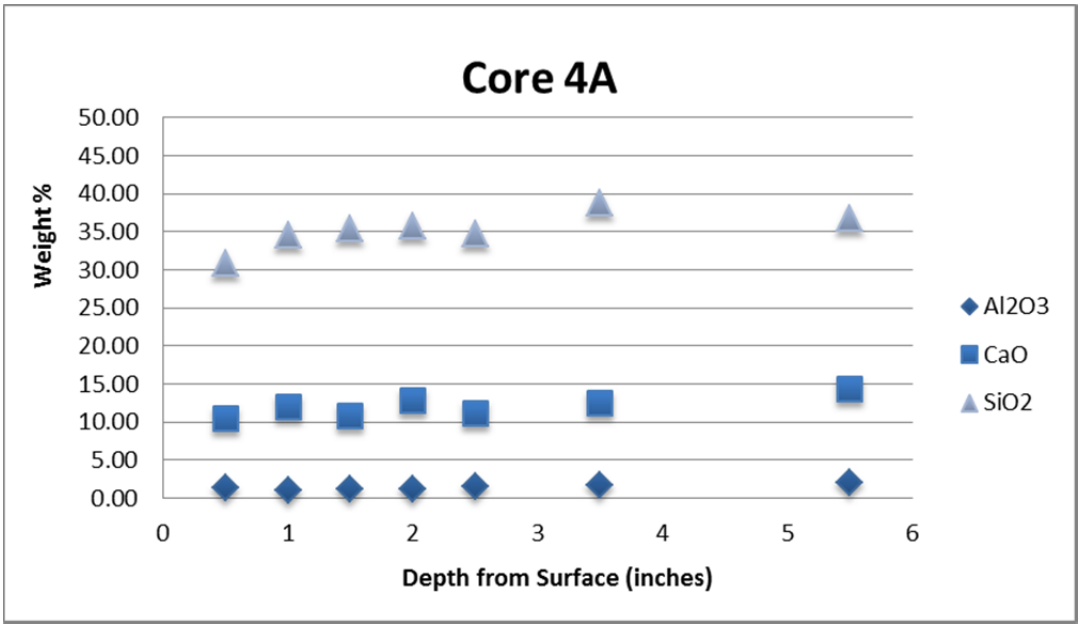

[a] The silica value in the sample at 2 inches in Core 1A is uncharacteristically low and most likely due to incomplete dissolution.

Figure 16: Concentration of Aluminum, Calcium and Silicon oxides as a function of depth beneath the surface for Core segment 4A.

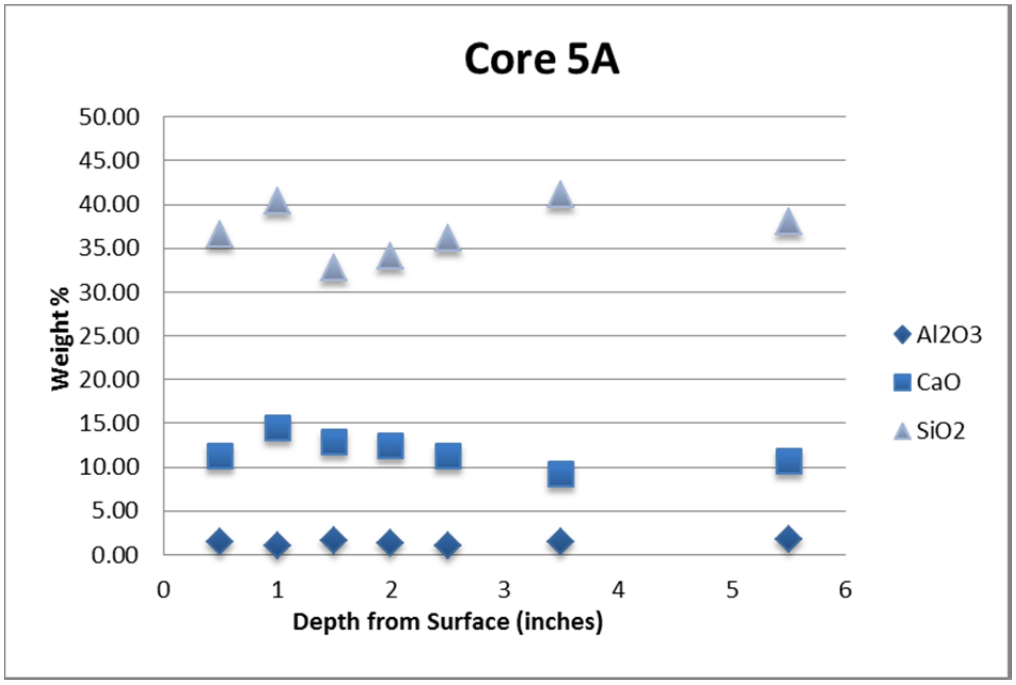

Figure 17: Concentration of Aluminum, Calcium and Silicon oxides as a function of depth beneath the surface for Core segment 5A.

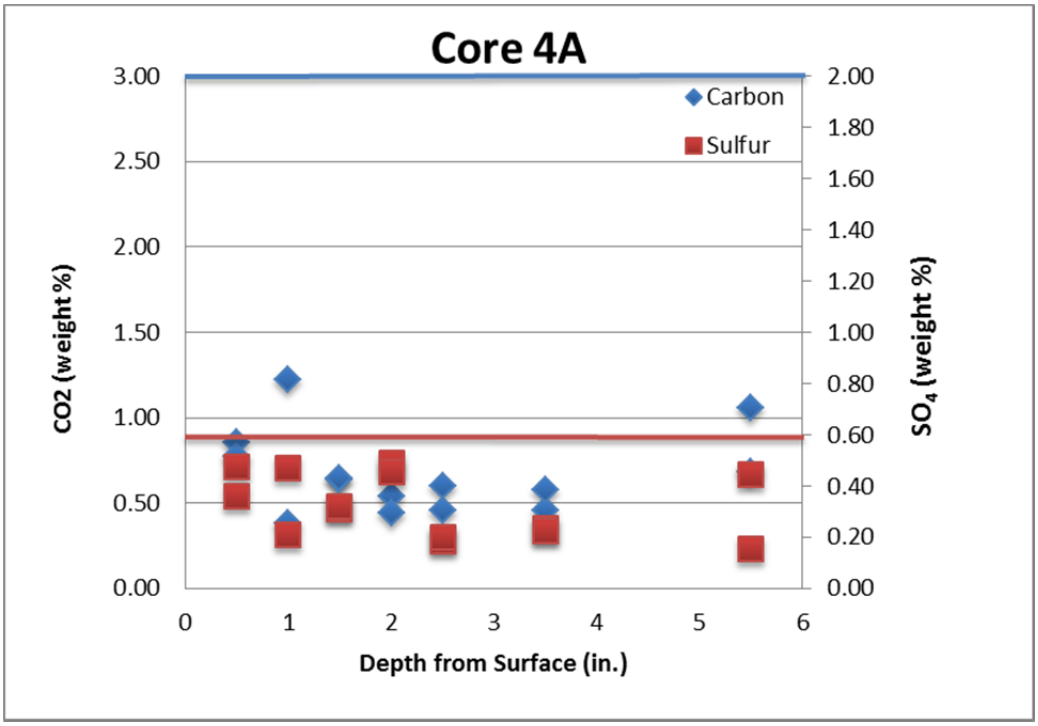

Figure 18: Sulfate and carbonate concentration in the interior core sample as a function of depth (horizontal lines are composition limits expected by mix design estimate and from ASTM C150 specification limit)

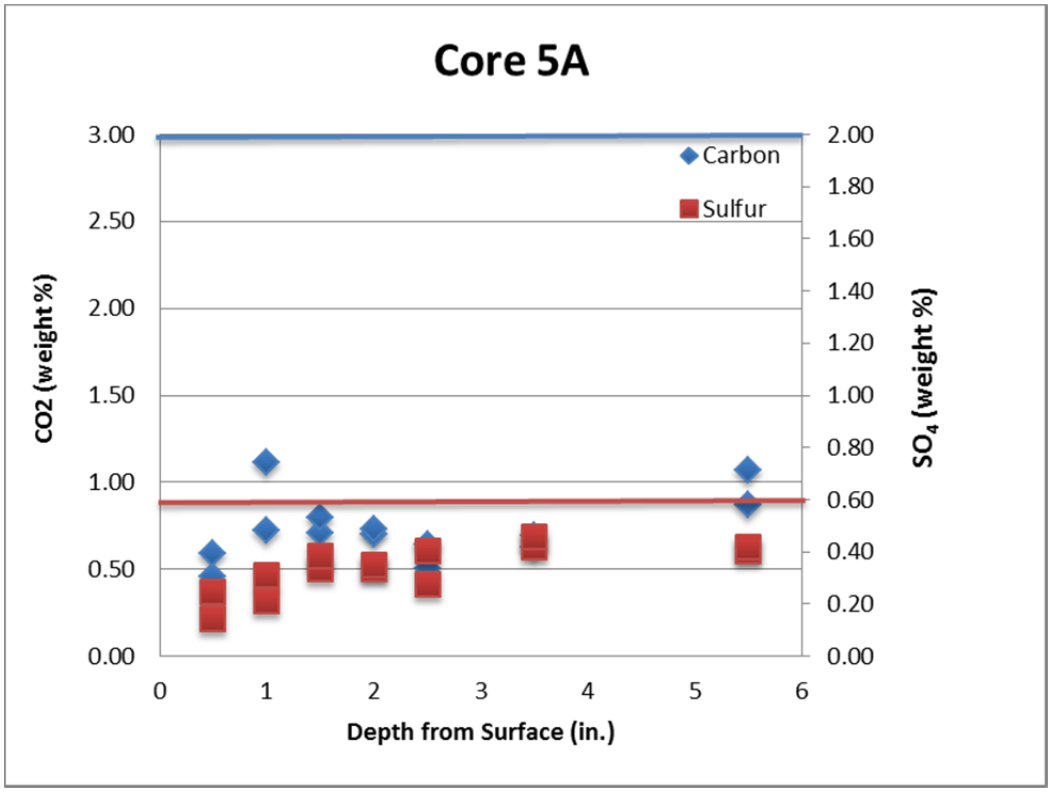

Figure 19: Sulfate and carbonate concentration in the interior core sample as a function of depth (horizontal lines are composition limits expected by mix design estimate and from ASTM C150 specification limit)

4.1.5 Volatile Species

The mass change (TGA) was conducted for 3 specimens as an independent determination of moisture, CO_2 and SO_2. The TGA curve indicates the weight percent (wt %) of volatile species in the concrete due to their decomposition in the sample as it is heated. The mass spectrometry curves correspond to the molecular weight of the individual compound with 18 atomic mass units (amu) corresponding to H_2O, 44 and 46 indicating CO_2 and 64 representing SO_2.

Figure 20, Figure 22 and Figure 24 show the weight loss for samples 5A-1A-3, 5A-1A-7 and 5A-1B-11 (see Table 2), respectively. Figure 21, Figure 23 and Figure 25 show the corresponding mass spectroscopy curves for Figure 20, Figure 22 and Figure 24, respectively. The mass spectrometry curves give indication as to which decomposition reaction is occurring. Initially, water comes off the sample at approximately 70 °C and 450 °C. These events correspond to dehydration of physical water and decomposition of portlandite ($Ca[OH]_2$). In between the two events, several other cementitious phases (e.g., ettringite) give up water and contribute to the weight loss of the sample as seen in Figures 20, 22 and 24. A modest increase in moisture content (4.5 – 6%) is observed as a function of depth when comparing Figure 20 to the other two figures. Additional weight loss occurs at 700 °C as a result of the

decomposition of calcite ($CaCO_3$), as indicated by the mass spectrometry signals at 44 and 46 amu (molecular weight of CO_2). Although no carbonation front (i.e., saturation of CO_2) was detected in any core samples (see section 4.1.1), the results indicate the presence of CO_2 in the cement phase near the surface. A decline in the magnitude of the weight loss as a result of CO_2 is observed as a function of depth. This is evident when considering the portion of the curves from 75-95 minutes (700 - 850 ºC) in Figure 22 through Figure 25. Finally, the mass spectrometry signal at 64 amu, corresponds to SO_2. Although a peak is clearly visible, no gradient in composition is visible as a function of depth. This may be because the levels of sulfur are too low to observe a gradient with this technique. These results are qualitatively consistent with the Leco analysis.

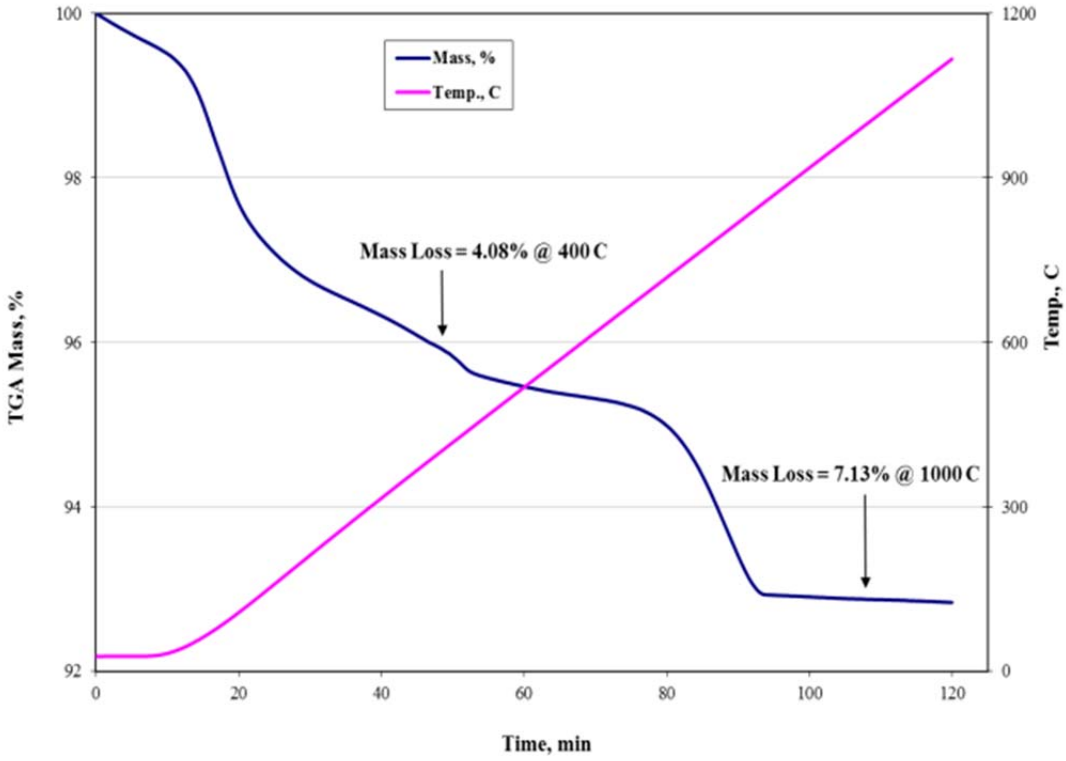

Figure 20: TGA curve for concrete sample 5A-1A-3 from 1 inch depth beneath the surface.

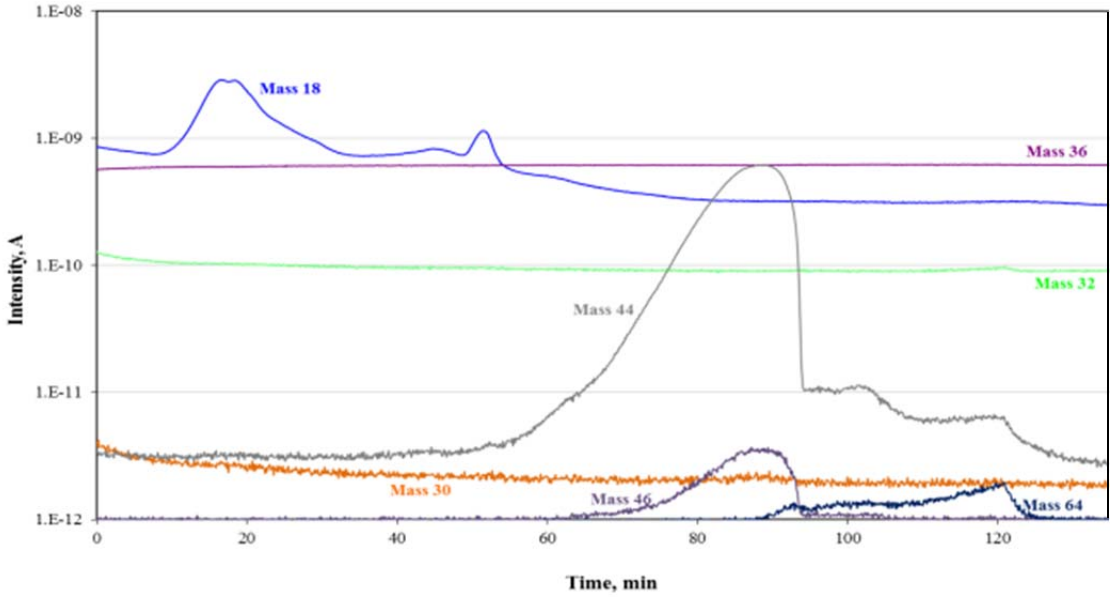

Figure 21: Mass spectroscopy curves for TGA curve for concrete sample 5A-1A-3 in Figure 20.

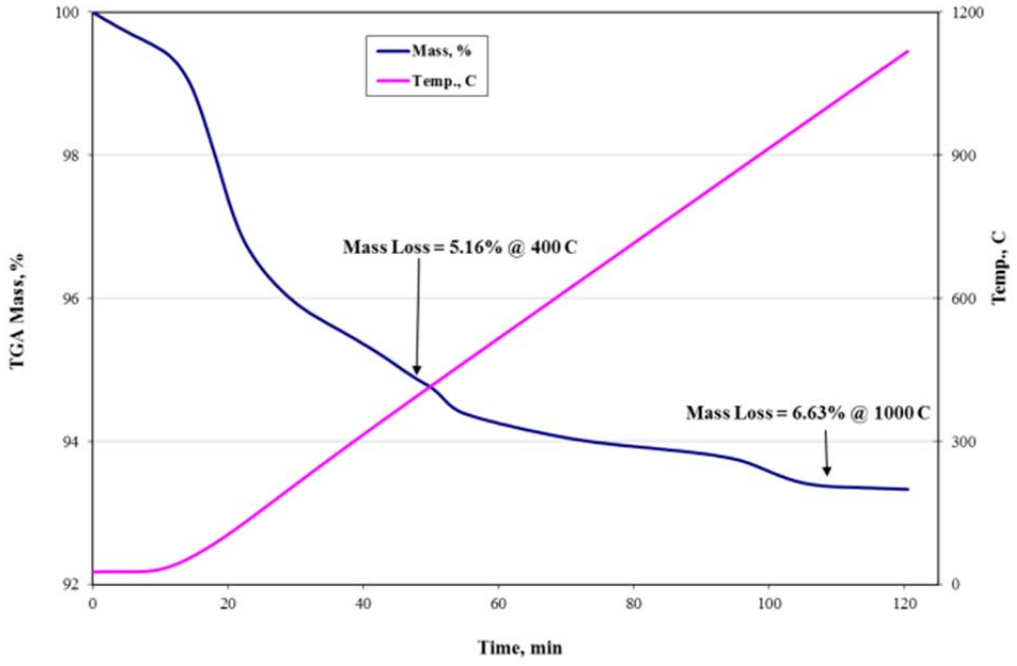

Figure 22: TGA curve for concrete sample 5A-1A-7 from 2 inch depth beneath the surface.

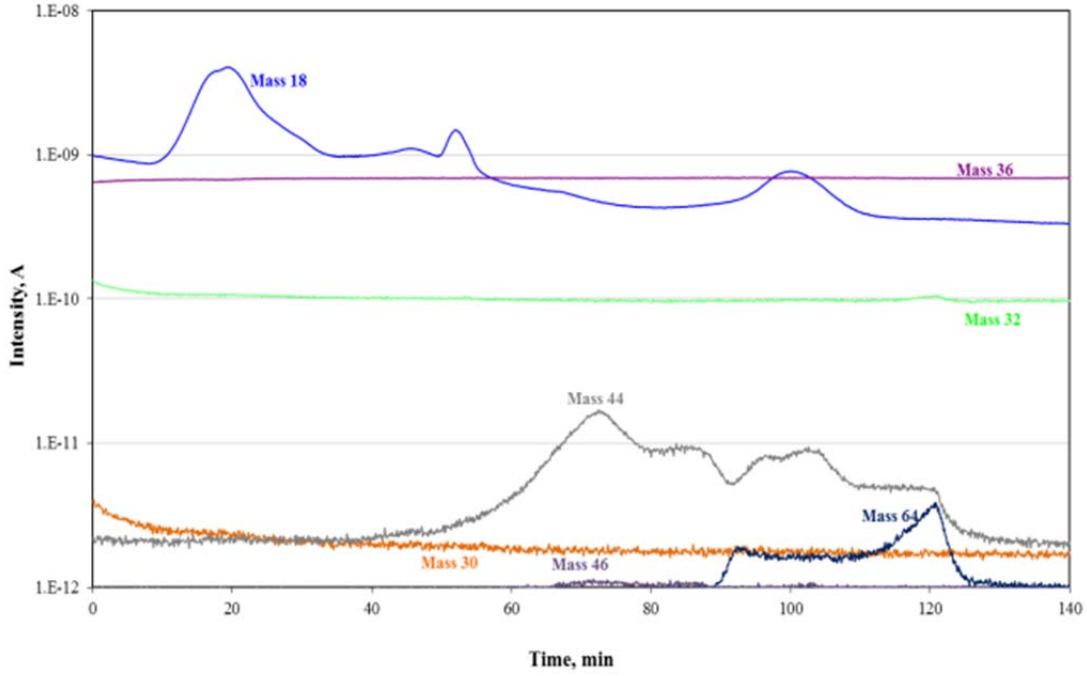

Figure 23: Mass spectroscopy curves for TGA curve for concrete sample 5A-1A-7 in Figure 22.

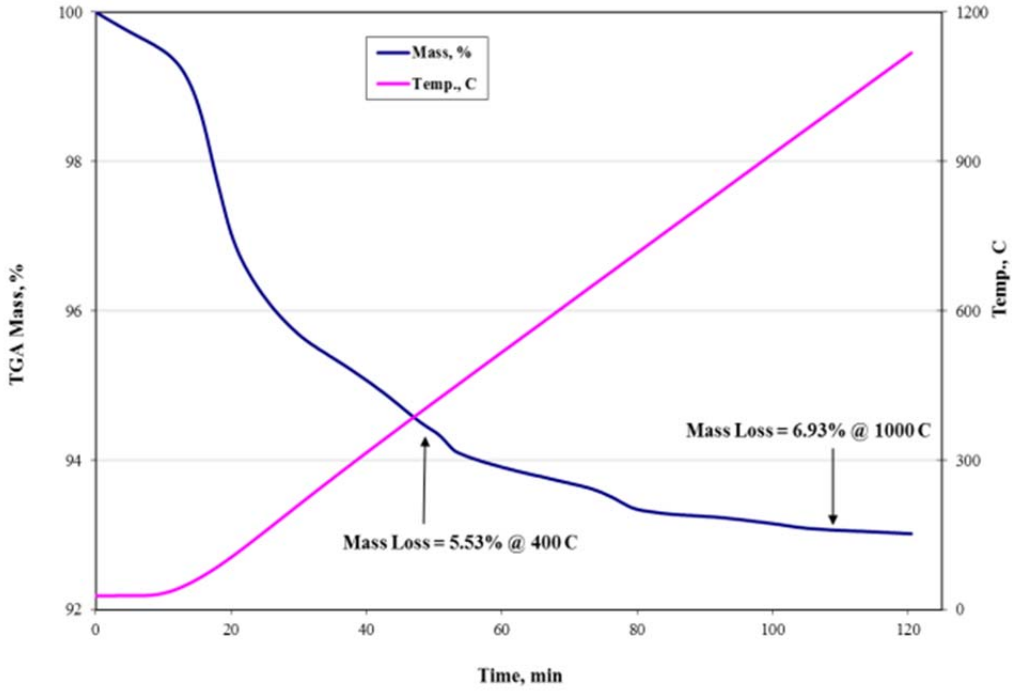

Figure 24: TGA curve for concrete sample 5A-1A-12 from 4.5 inch depth beneath the surface.

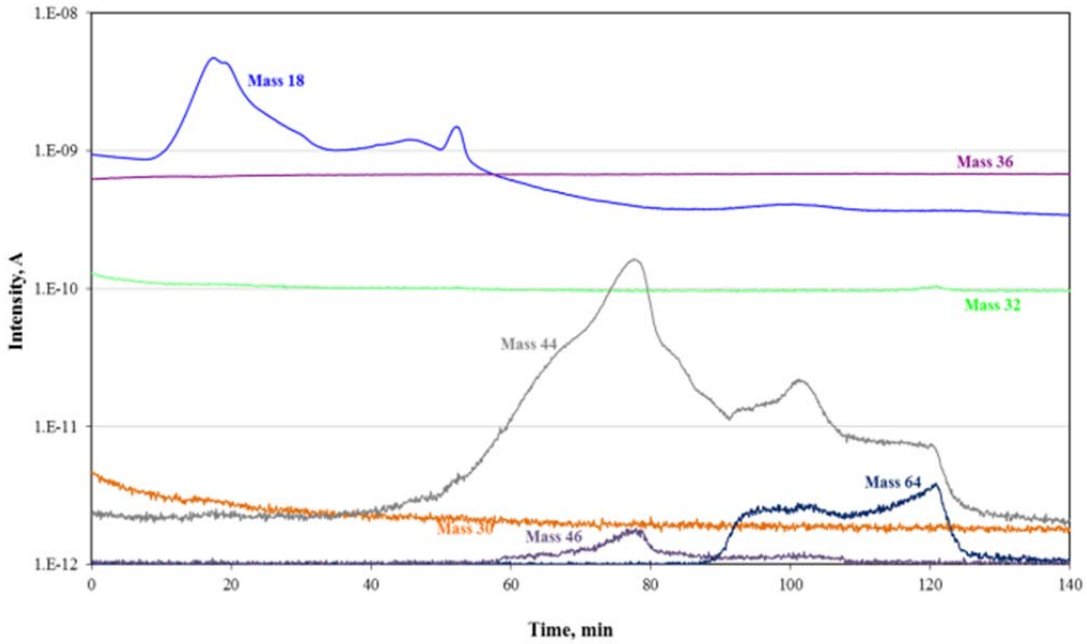

Figure 25: Mass spectroscopy curves for TGA curve for concrete sample 5A-1A-12 in Figure 24.

4.2 Interior Core Segments

The internal portions of each core had been sectioned into 3 segments for compression testing. After compression testing, the samples were examined to ensure valid loading configuration and compare the microstructure to the near-surface segments. The results from these analyses are contained in this section.

4.2.1 Compression Testing

The compression tests were performed in compliance with ASTM C 1231.[17] Segments 1C, 4C and 5C were 5.6 inch X 11.3 inch long, having an aspect ratio of approximately 2. The loading curves are presented in Figure 26 - Figure 28, for segments 1C, 4C and 5C, respectively. Three compression tests were performed and the three values of compression testing are summarized in Figure 29. The maximum load prior to failure was used to calculate the breaking strength. In every case, the actual breaking strength exceeded the specified compression strength (i.e., 2500 psi) by at least 1200 psi. This is expected since strengthening of concrete over time after placement is well documented in literature. Therefore, any degradation that has occurred is not yet significant enough to have any effect on the structural integrity of the concrete.

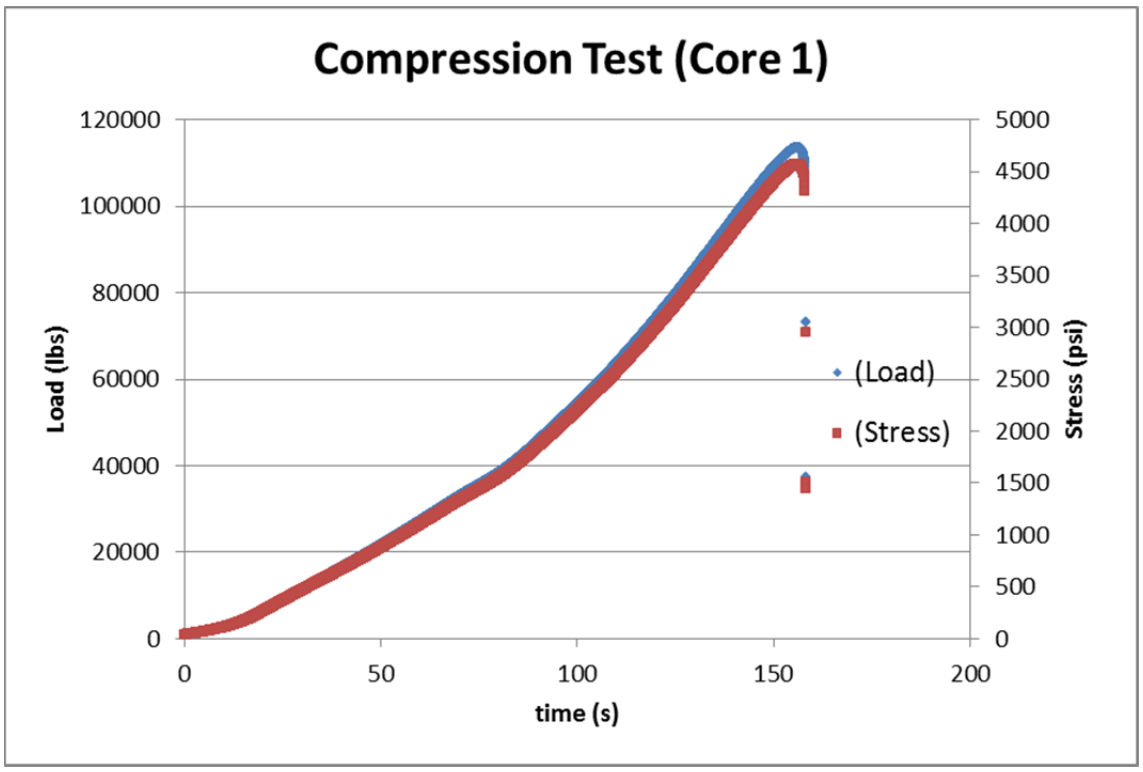

Figure 26: Load/Stress vs time for the compression test of Core 1C.

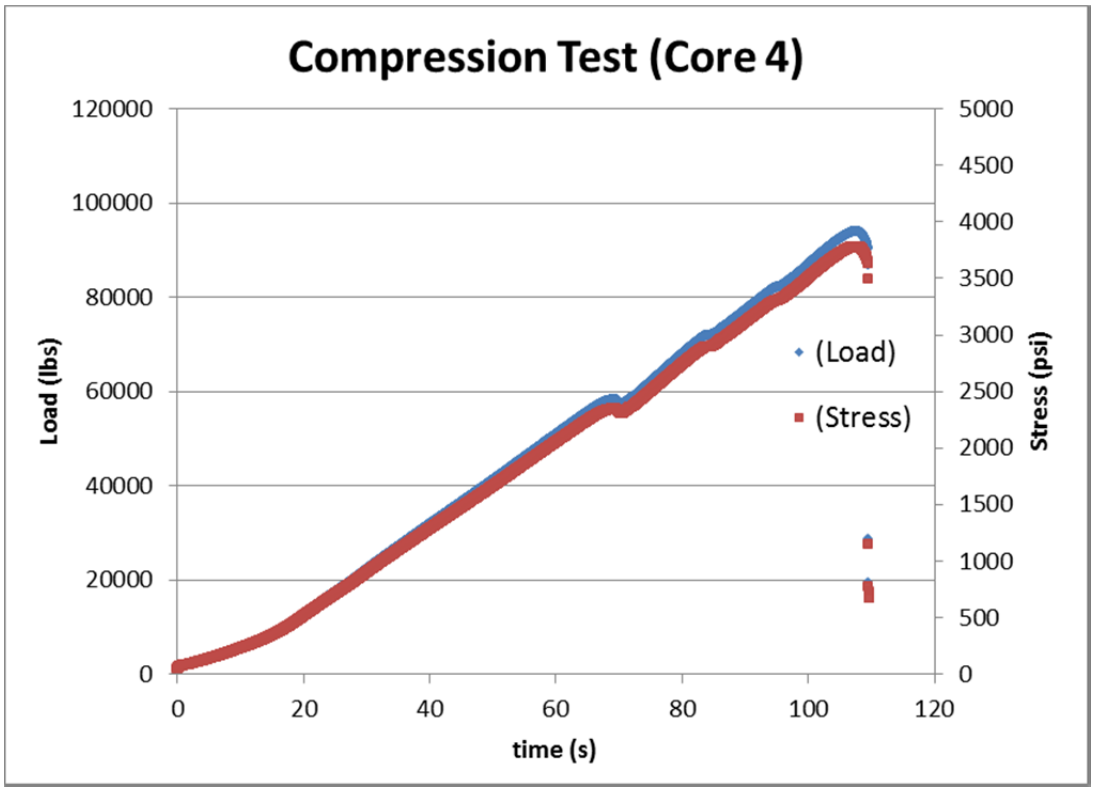

Figure 27: Load/Stress vs time for the compression test of Core 4C.

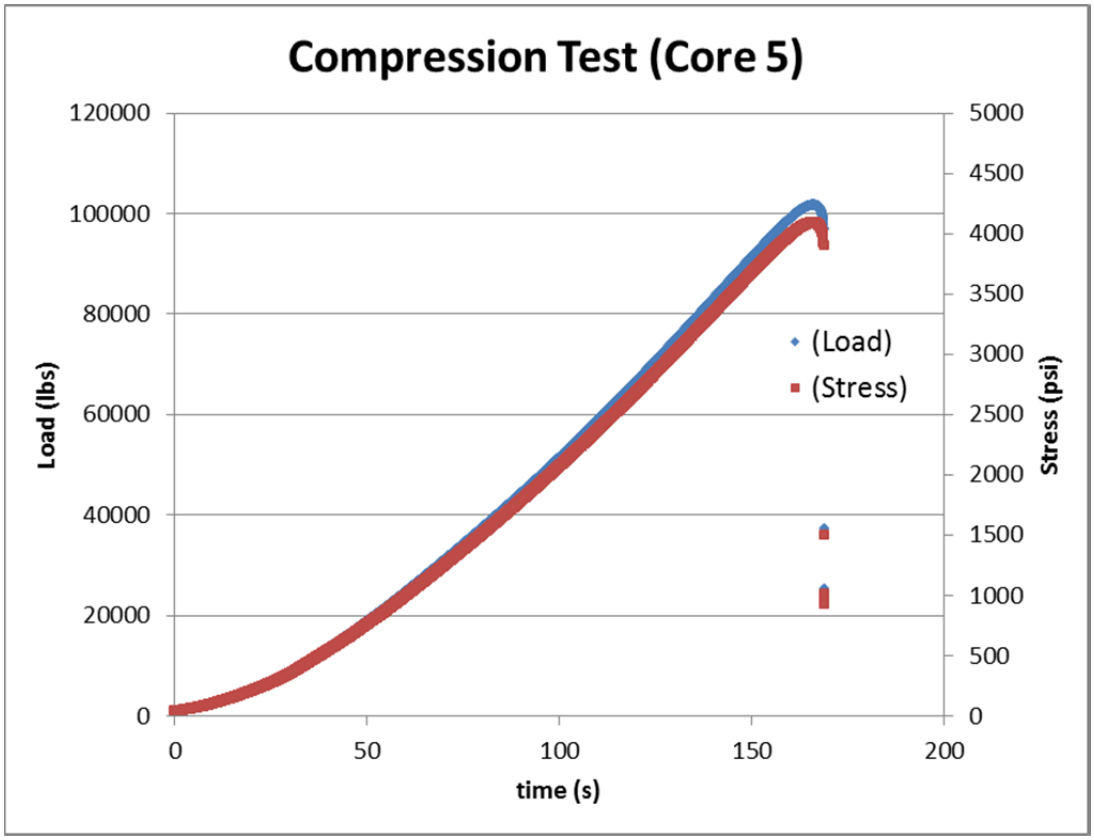

Figure 28: Load/Stress vs time for the compression test of Core 5C.

The compression tests results are interpreted using the technical guidelines ACI 214R-11 from the American Concrete Institute. [20] In general, a sufficient number of tests are needed to accurately indicate the variation of the concrete strength and permit application of appropriate statistical procedures for interpreting the results. When a sufficient number of tests are not possible, the guide recommends that the required average compressive strength (f_{cr}') should exceed the specified compressive strength (f_c') by a factor in order to provide confidence that the true average strength will not fall below the specified strength. In the case of 2500 psi concrete, the factor recommended is 1000 psi.

$$f_{cr}' = f_c' + 1000 \text{ psi}$$

Hence, the average value of compressive strength (f_{cr}') must exceed the 3500 psi to be acceptable. Figure 29 presents the current compressive data set with a line marking both *fc'* (solid) *and fcr'*(dashed). All test results exceeded this required value. An average value of 4148 psi was determined for the sample set which also exceeds the value of 3500 psi. Hence, the concrete has maintained this minimum required strength value. Any degradation processes that have been discussed at present should not significantly affect the structural integrity of the concrete. Therefore, a change to the property inputs for concrete to the structural analysis should not be necessary.

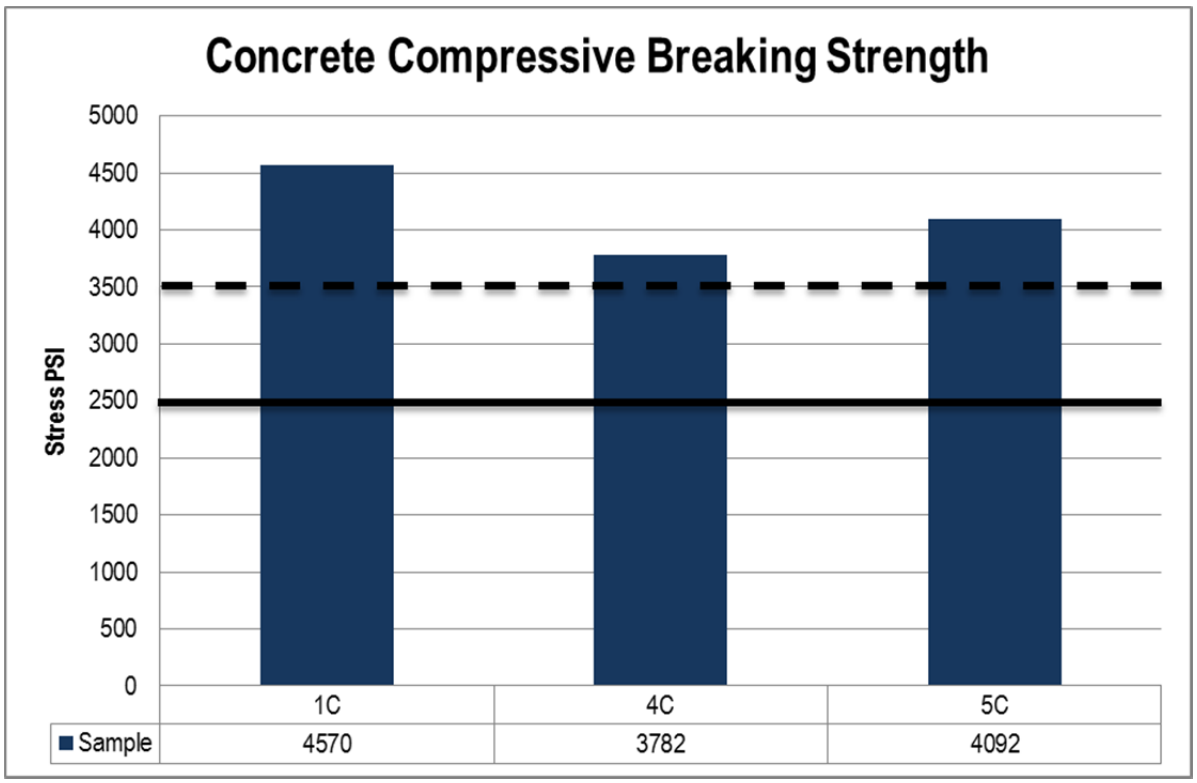

Figure 29: Compression test results from concrete test cylinders with the specified minimum design strength[8] (solid line) and recommended minimum average compression strength[20] (dashed line).

4.2.2 SEM Microanalysis

The interior core segments from C basin were examined after the compression tests. Samples were removed from area of the compression test specimen (i.e., top middle and bottom). The BSE micrographs representative of the microstructure in each sample are presented in Figure 30 through Figure 38. Phases are labeled where EDS data effectively identified the composition of phases present. As in the case of the near surface specimens, the wide spread presence of ettringite is clearly visible throughout the samples. Other phases present were consistent with the near surface specimens (i.e., microcline, iron oxides, ilmenite and quartz). Zircon ($ZrSiO_4$) and ilmenite ($FeTiO_3$) were also present. This is consistent with aggregates used in structural concrete. Alkali-silica gel was not observed to be prevalent in the structure. Figure 39 shows the results of a typical line scan which would detect the formation of reactive gel at the aggregate/cement paste interface. The presence of microcracking was noted but did not appear to be prevalent within the aggregate phases (see Figure 40). Rather, the cracking spanned from aggregate to aggregate through the cement paste phase. Since these samples were obtained from post-test characterization of a failed cylinder, some of these cracks may have been a result of the compression test. These observations indicate that degradation beneath the surface of the concrete in C area should not be a concern.

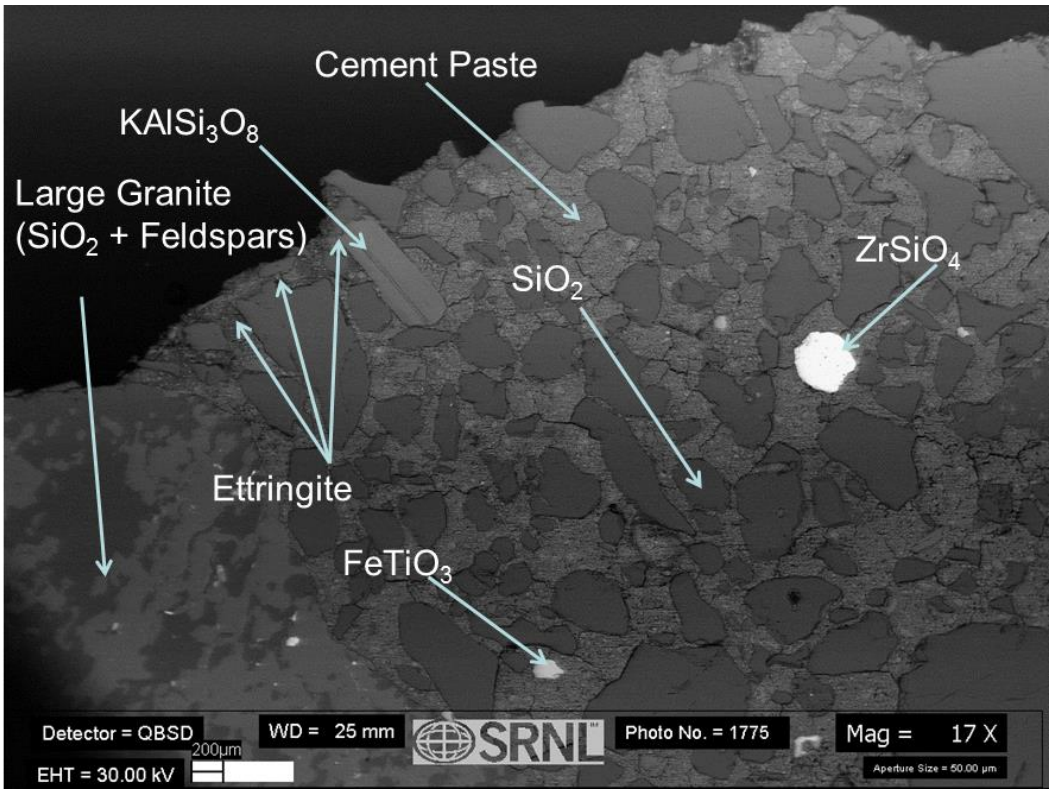

Figure 30: SEM backscattered electron photomicrograph of compression specimen 1C (top).

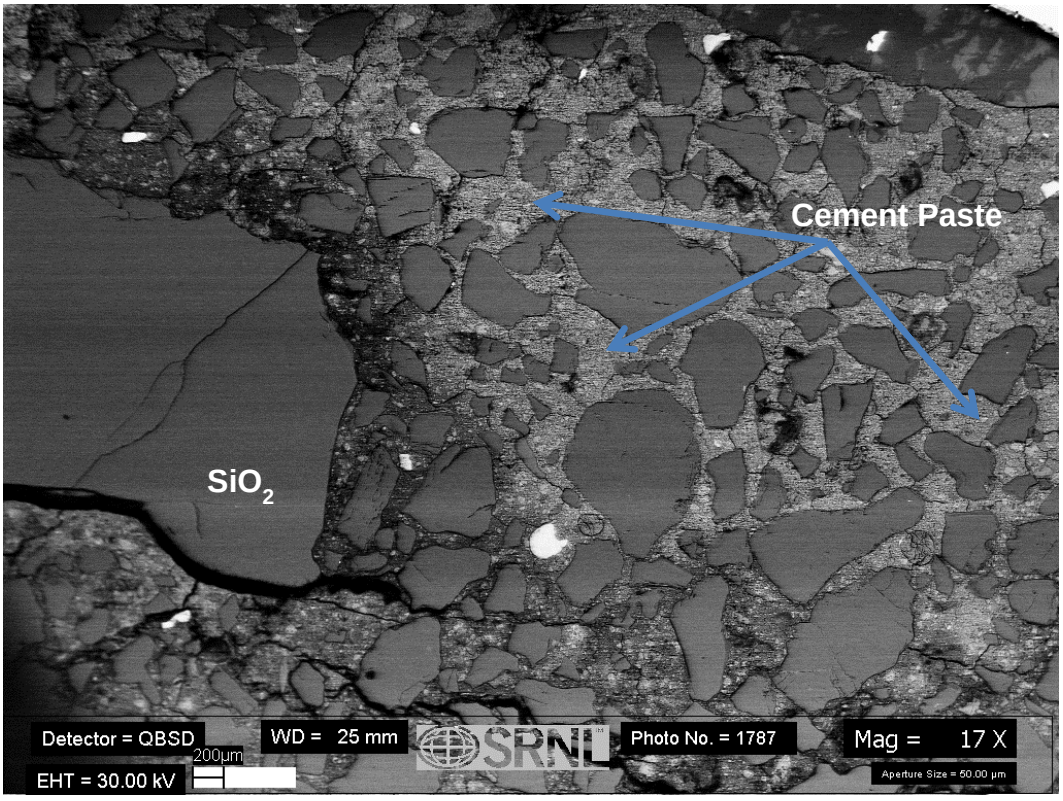

Figure 31: SEM backscattered electron photomicrograph of compression specimen 1C (middle).

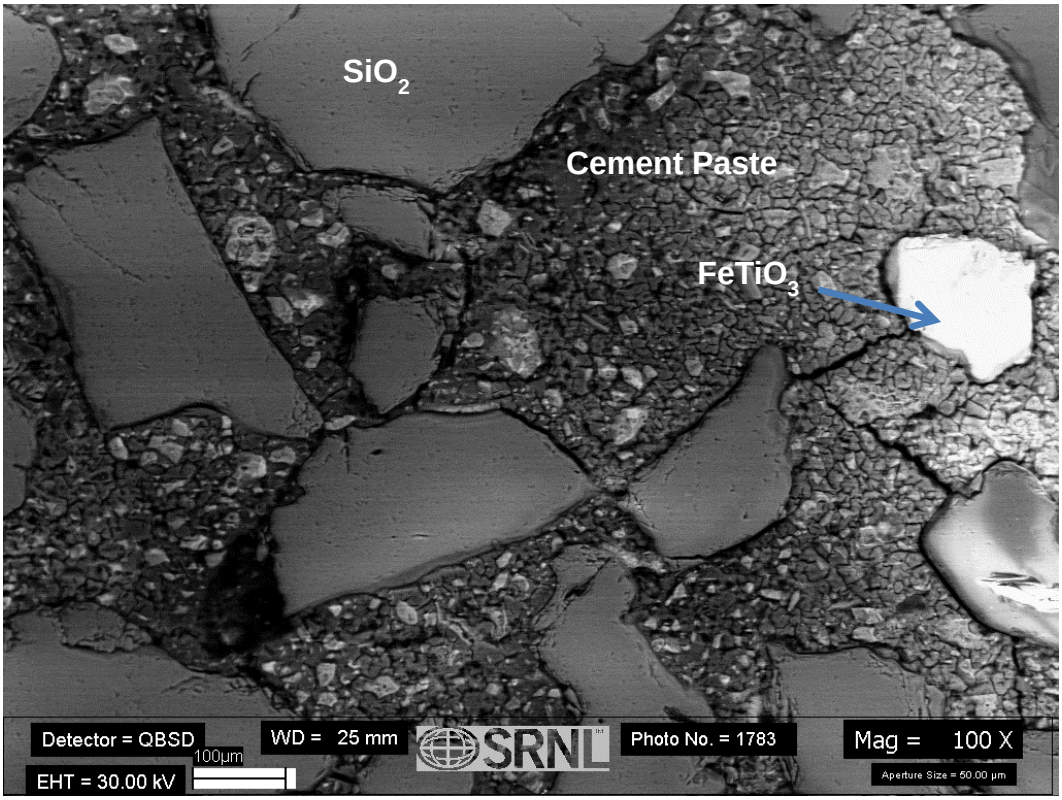

Figure 32: SEM backscattered electron of compression specimen 1C (bottom).

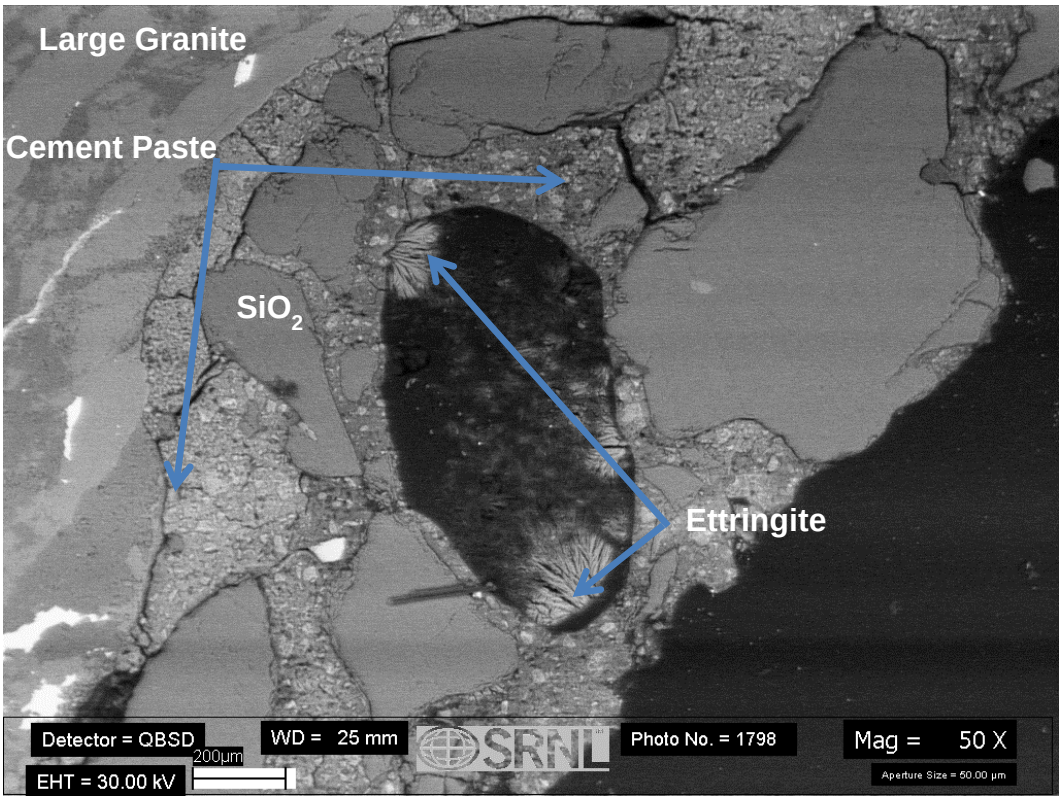

Figure 33: SEM backscattered electron photomicrograph of compression specimen 4C (top).

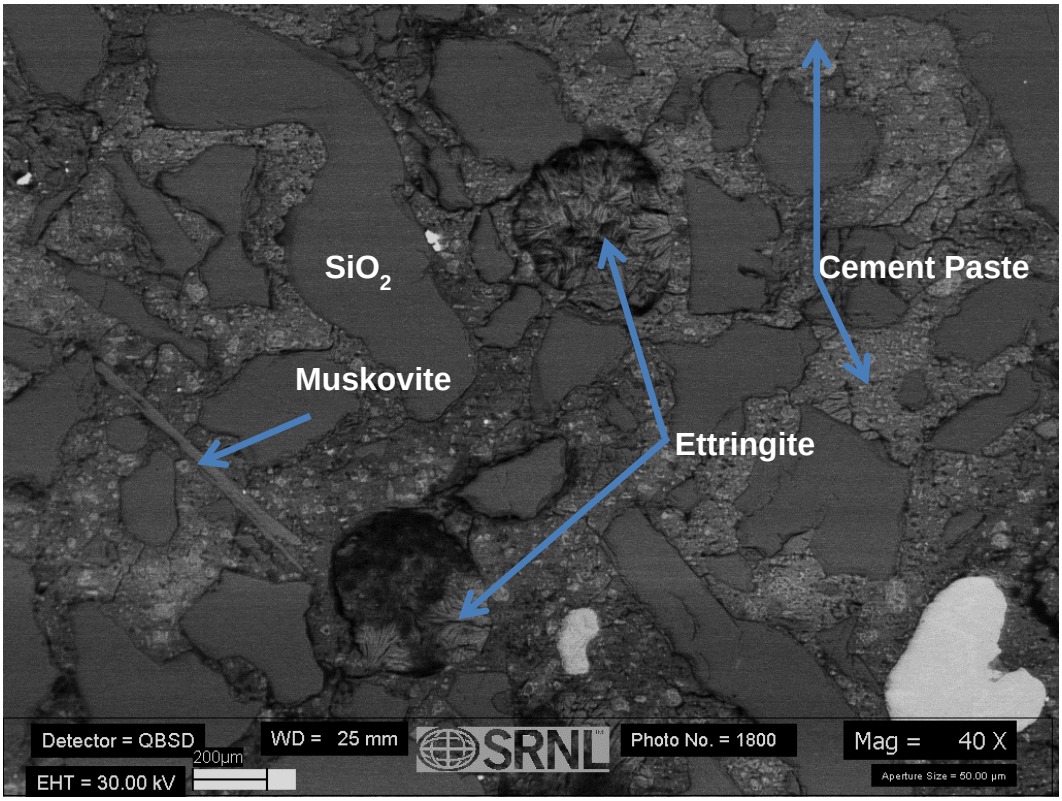

Figure 34: SEM backscattered electron photomicrograph of compression specimen 4C (middle).

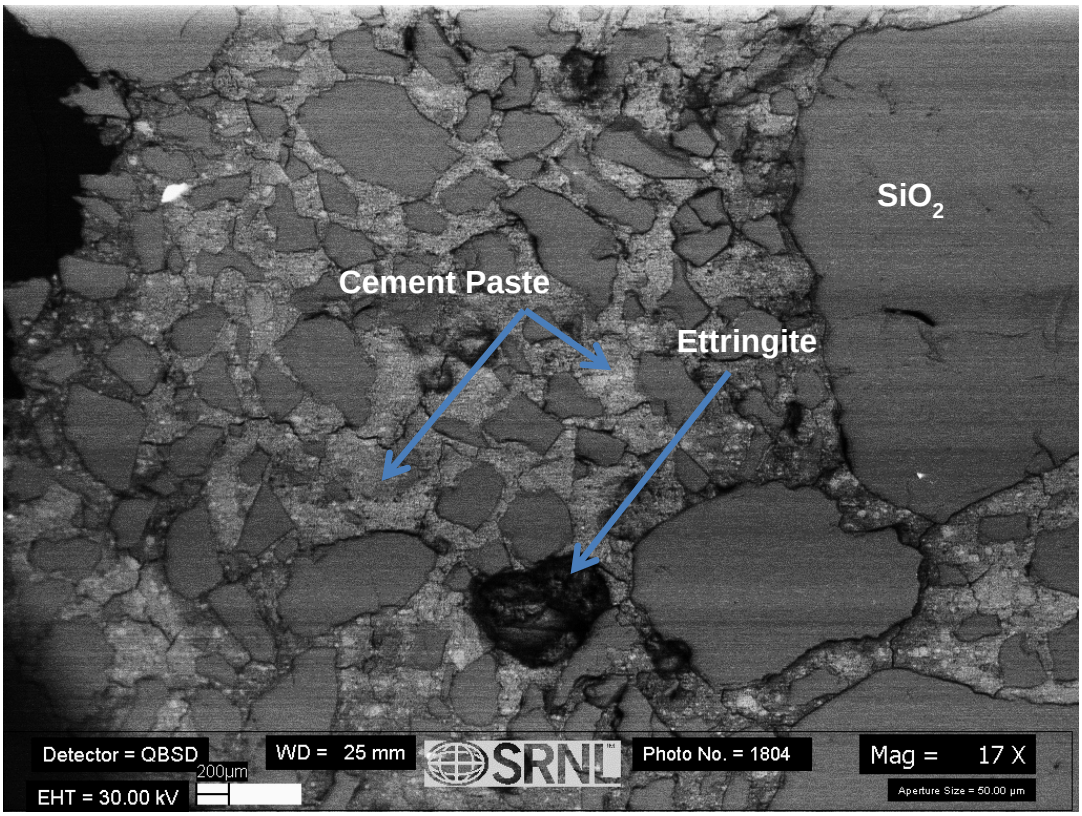

Figure 35: SEM backscattered electron photomicrograph of compression specimen 4C (bottom).

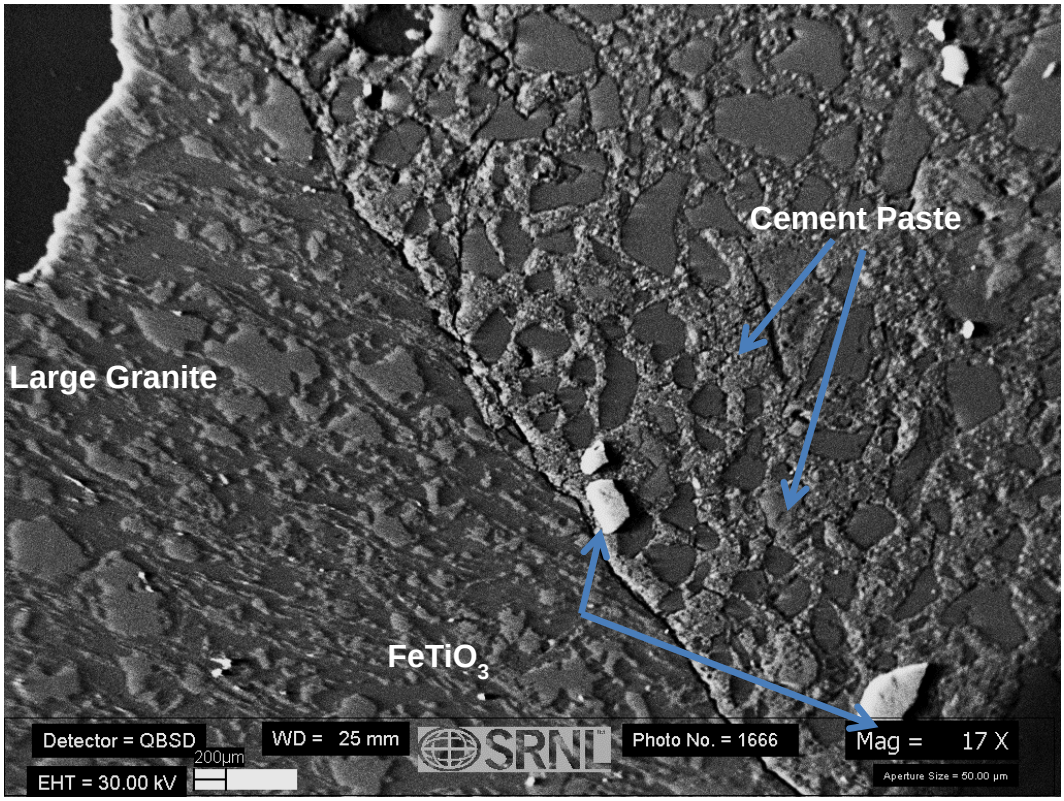

Figure 36: SEM backscattered electron photomicrograph of compression specimen 5C (top).

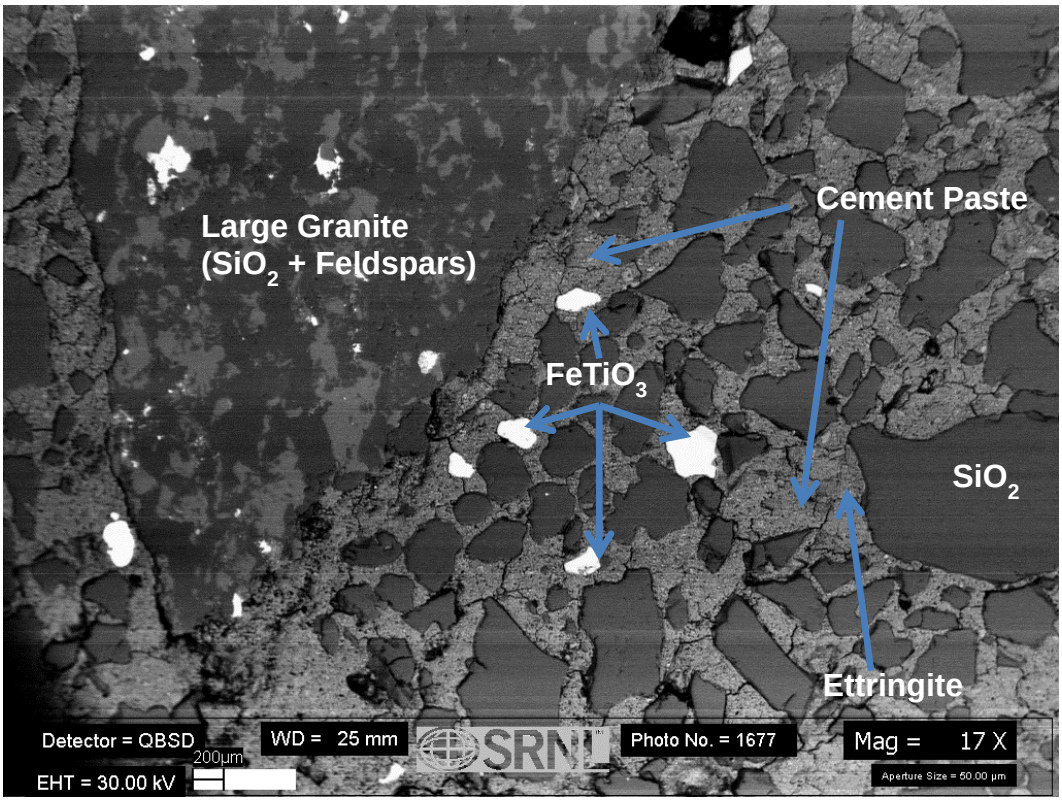

Figure 37: SEM backscattered electron photomicrograph of compression specimen 5C (mid).

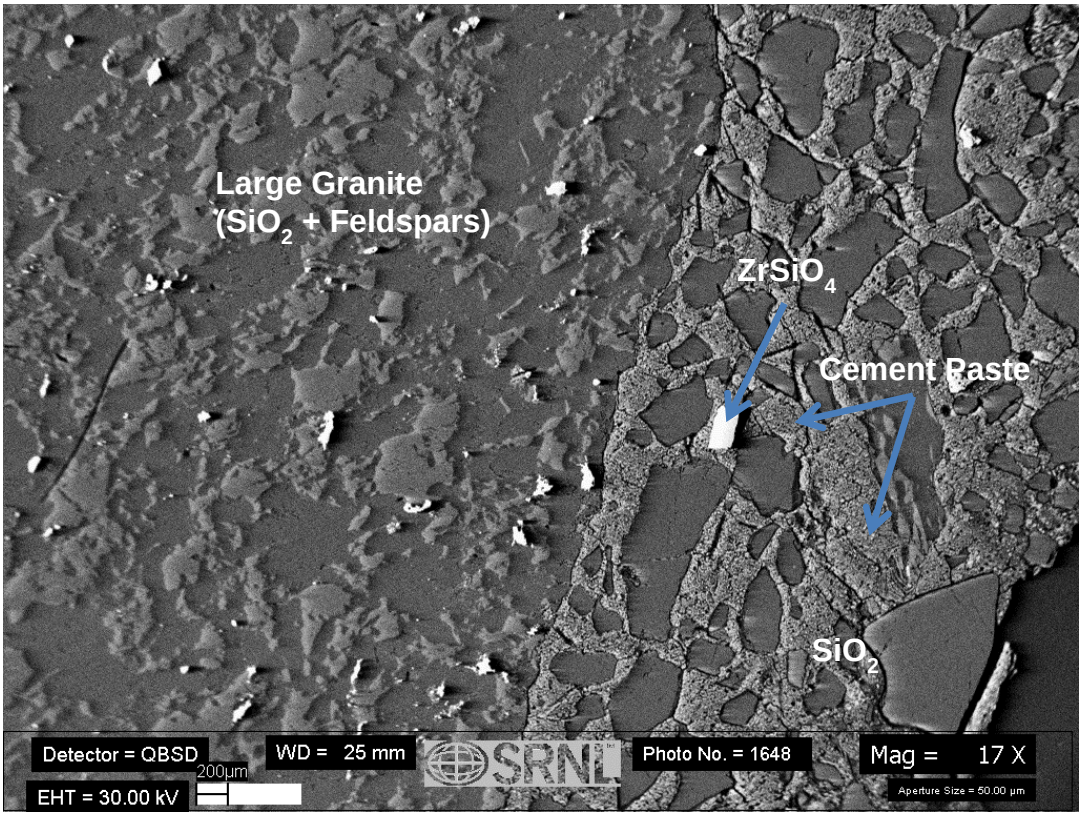

Figure 38: SEM backscattered electron photomicrograph of a cross-sectioned sample from compression specimen 5C-bot.

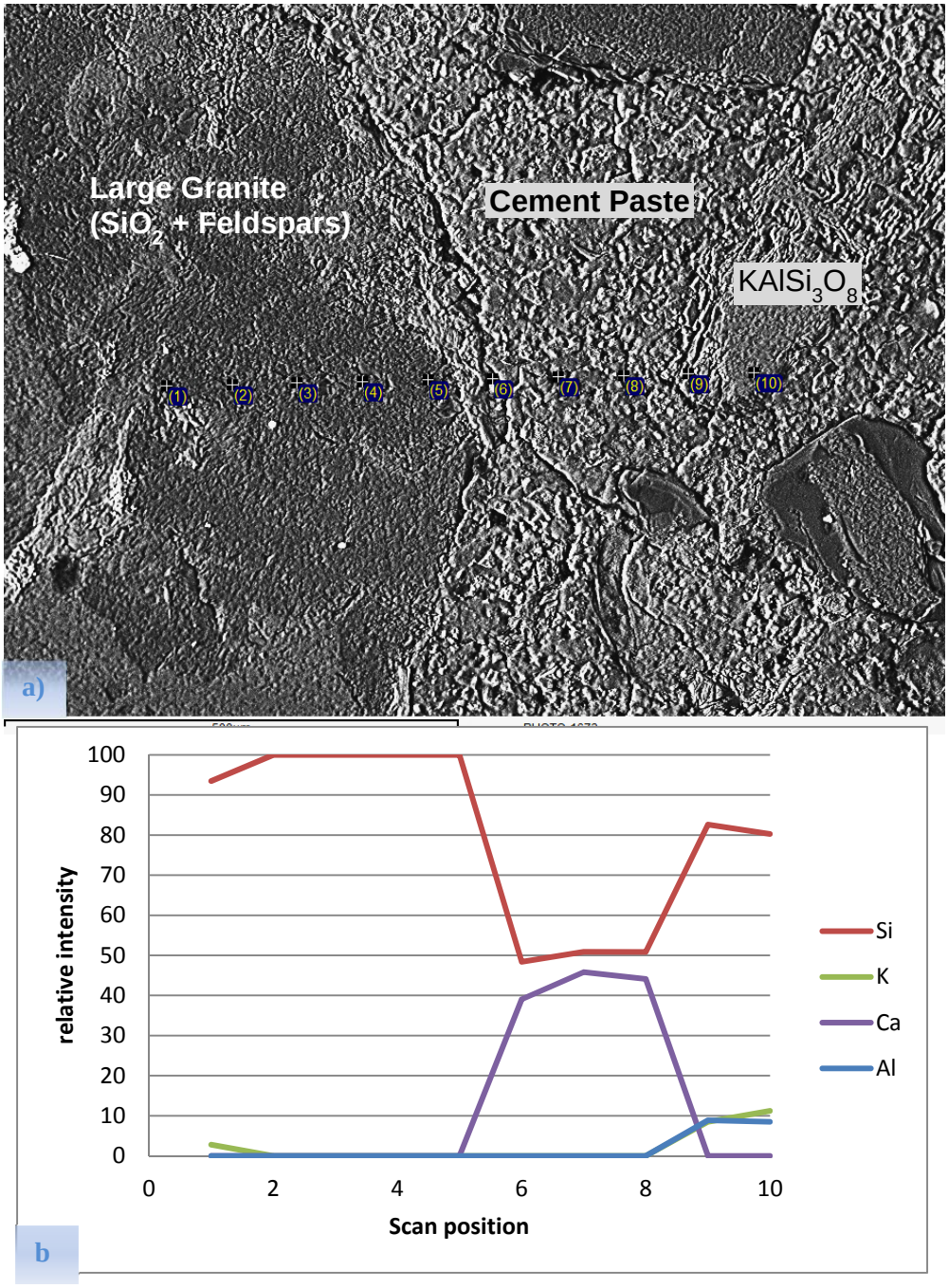

Figure 39: Line scan of 5C top showing the chemical transitions between large granite, cement paste and small aggregate phases

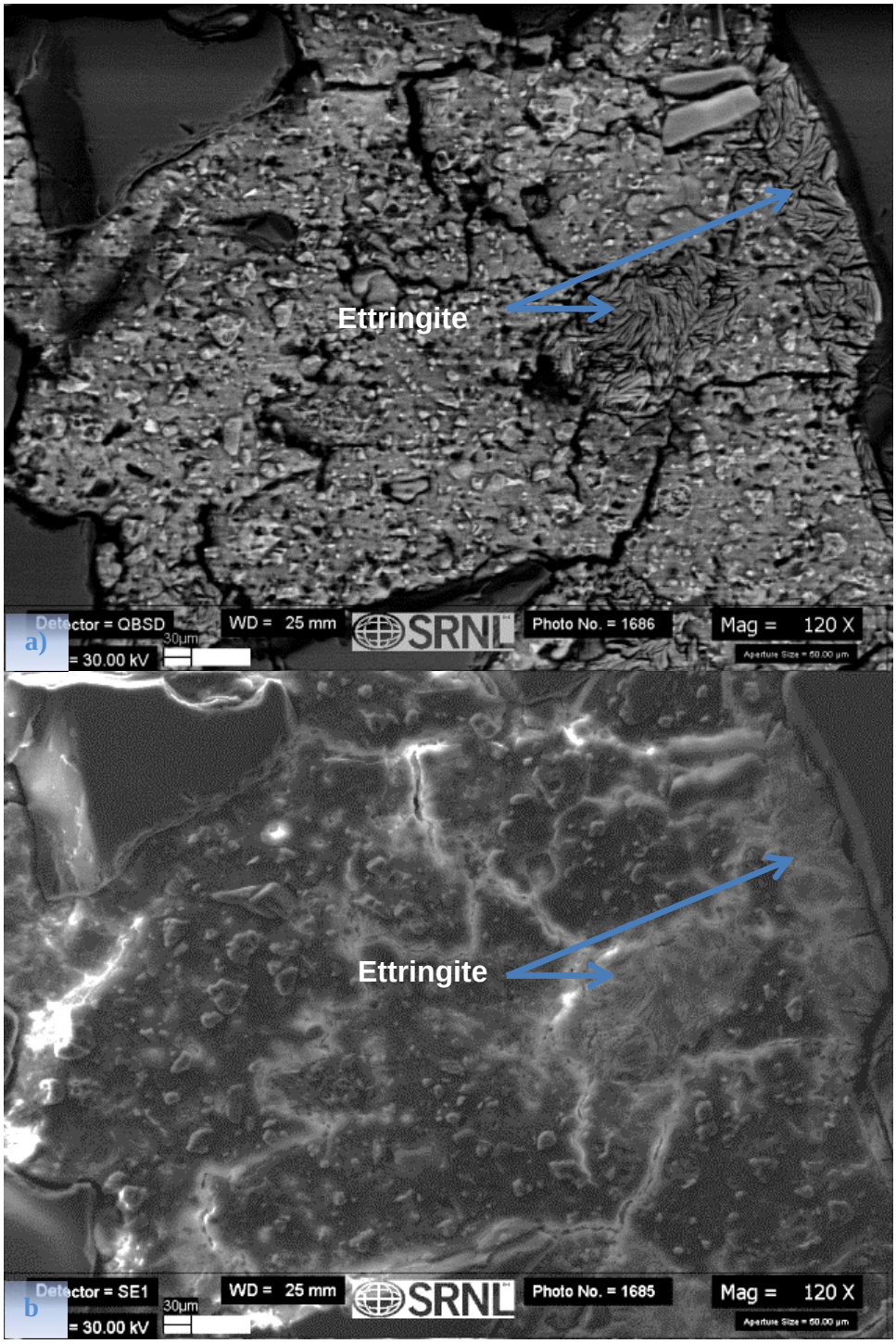

Figure 40: Micro-cracking and ettringite formation in the cement paste phase of sample 5C middle. Backscatter (a) and secondary electron images (b).

5.0 Conclusions

Concrete core samples from C basin were characterized through material testing and analysis to verify the design inputs for structural analysis of the L Basin and to evaluate the type and extent of changes in the material condition of the concrete under extended service for fuel storage.

The microstructure and chemical composition of the concrete exposed to the water was profiled from the water surface (excluding the first 0.5 inch) into the wall to evaluate the impact and extent of exposure. No significant leaching of concrete components was observed. Ingress of carbonation or deleterious species was determined to be insignificant. Phases in aggregates were identified and characterized. No evidence of alkali-silica reactions (ASR) was observed.

Ettringite was observed to form throughout the structure (in air voids or pores), however the sulfur content was measured to be consistent with sulfur content allowed by the building specification[8] used to construct the facility. Similar ettringite trends were observed in the interior segments of the core samples. Limited micro-cracking was observed throughout the structure which could be a symptom of delayed ettringite formation (DEF) but did not appear significant.

The compressive strength of the concrete at the mid-wall of the basin was measured, and similar microstructural analysis was conducted on these materials post compression testing. The microstructure was determined to be similar to near-surface segments of the core samples. The average strength was 4148 psi, which is well-above the design strength of 2500 psi. The analyses showed phase alterations and minor cracking in a microstructure did not affect the design specification for the concrete.

This work has been applied to validate the material property inputs for structural analysis of the L basin.[21-22] Currently, no change to property inputs is necessary due to the adequate margin of compressive strength measured and the absence of detected degradation processes.

6.0 Path Forward Recommendations

This study focused on testing and analysis to quantify aging effects on the bulk concrete and the water contact region of the basin. The work did not explicitly address the following additional features of the L Basin concrete structure and the potential degradation phenomena that can cause weakness in the basin structure:

- Carbonation of above grade concrete[13] to potentially weaken the concrete structure
- Degradation of exterior surface of concrete structure below grade from ground water infiltration
- Degradation of the waterstops that could allow out-leakage of basin water to the L building interior or to the environment
- Degradation of local regions including rebar/concrete interfaces associated with active leak sites that could weaken the rebar functions within the concrete

Carbonation of concrete in contact with air-exposed regions were recently investigated with tests at P-reactor building before its closure. These concrete results should have general applicability to the L Basin above-grade structure. It is recommended to formally evaluate the concrete material and service

conditions from P-reactor building concrete test results, and their applicability to L Basin concrete, with a follow-up of recommended prescriptive verification tests, if warranted post comparisons.

General activities to validate the long-term integrity of the L basin structure to perform its intended safety function for an extended storage mission are discussed below.

6.1 Exposure of concrete to groundwater

Groundwater in contact with concrete is an aging condition for concrete. An example of a specific degradation mechanism for this exposure condition is the ingress of sulfates from soil, and that impact includes formation of the deleterious ettringite phase.

The present work has shown that water contact did not significantly alter the composition and impact the condition of the basin concrete. It is noted that the basin water was essentially at high quality or a "pure condition."

It is recommended that evaluation of the soil adjacent to the L Basin be characterized for sulfate content and the results evaluated for potential degradation of the concrete in contact with groundwater.

6.2 Degradation of Waterstops

Waterstops were used at construction joints in the fabrication of the L Basin. The construction specification listed allowable materials to be neoprene elastomer, copper, stainless steel or other material.[23] The intended function of the waterstops is to preclude seepage in the event of potential cracking of the concrete at the location of the construction joint. As noted below, cracking does not necessarily impact the structural integrity of L Basin, and L Basin has seepage at present.

It is recommended that an evaluation of the potential loss of function due to aging of each of the allowable materials for waterstops in L Basin be investigated at or near the established existing or historical leak sites.

6.3 Cracking leading to leak sites in the structure and impact on basin integrity

Cracking of the concrete will occur from shrinkage during concrete curing and/or settlement. Freeze-thaw cycling can also cause cracking. Cracking in reinforced concrete structures such as the L Basin concrete structure does not necessarily diminish its structural capacity. However, the potential impact of cracks that are dry, moist or intermittently wet could lead to: 1) calcium leaching; 2) provide a short-circuit pathway for chloride ingress and/or carbonation; and 3) facilitate corrosion of the steel rebar matrices causing gross and/or localized degradation including concrete spallation and loss of rebar function. It is suggested that non-radiological concrete samples at or adjacent to moist or historical leak sites should be taken and analyzed for extent of degradation and graded for deleterious species infiltration potential.

Non-destructive examination methods for cracked concrete and inspections to better quantify the extent of L Basin cracking and the potential regions of localized attack should be pursued. Untested, remaining C Core sample specimens that have rebar/concrete interfaces could be used to investigate rebar/concrete interactions in cracked concrete structures in conjunction with NDE techniques. Induced corrosion and

NDE inspection could be correlated to create a benchmark for field inspections to supplement the SIP. It is recommended that these core segments be reserved for this type of pilot testing.

6.4 Application of C Basin concrete results to L Basin concrete

The current test program involved the concrete material source from C Basin. The C Basin concrete was used because it was readily available with the in-situ disposition of the basin. It is expected to be reasonably representative of the concrete and the aging conditions experienced by the L Basin concrete structure. A verification sampling and testing of the L Basin concrete would strengthen the application of the results from the C core analysis baseline. The scale of this sample could be a small core of L area concrete from the below grade structure to compare to C area concrete. A test plan would be designed to create an L basin sample matrix to provide a basis of comparison for the microstructure, composition and profile of deleterious species with respect to C basin.

6.5 Remaining C Basin concrete material

Available material not tested in this present test and analysis campaign includes 12 more C basin core segments that are suitable for compression testing and 2 near surface cores that are in interim storage. Additional testing under the same conditions is not recommended, based on the results. It is recommended that these materials be kept in long-term, archival storage until such time that the test plan is re-evaluated or a new test plan is prescribed. The current storage facility meets all requirements of a level "A" storage facility[24] and it will suffice for long term storage with the addition of a specimen log to ensure the traceability of each specimen is maintained and the testing is documented. In addition, the plastic bags used for storage will be inspected to ensure they are leak tight.

Accelerated aging of concrete is often used to predict degradation of properties in the future or end of service life condition. It is recommended that the remaining compression test cylinders be utilized to explore accelerated aging methods for concrete to confirm the expected strengths of L Basin concrete throughout the duration of its proposed extended service life.

7.0 References

[1] 105-L Structural Integrity Information Sheets, WSRC-TR-2005-00303, Rev. 3, Westinghouse Savannah River Company, Savannah River Site, Aiken, SC.

[2] WSRC-TR-2008-00202, "L Basin Life Expectancy," Washington Savannah River Company, July 2008

[3] Technical Memorandum # SRNL-MST-2006-00016, From: A. J. Duncan, To: C. E. Olson, Subject: Technical Justification for the Core Sampling of the Selected Areas of L area Basin, June 29, 2006.

[4] SRNL-STI-2011-00190, Demonstration of Long-Term Storage Capability for Spent Nuclear Fuel in L Basin, Savannah River Nuclear Solutions, April 2011

[5] SRNL-TR-2011-00320 Rev. 0, "Activity Plan for L Basin Materials Surveillance and Structural Integrity Evaluation," Savannah River National Laboratory, Savannah River Nuclear Solutions, Aiken, SC, 29808, December, 2011.

[6] SRNL-TR-2012-00228, "Core Sampling of Concrete from C Basin in support of L Basin Extended Service," A.J. Duncan, Savannah River Nuclear Solutions, Aiken, SC, 29808, September 2012

[7] Technical Memorandum # SRNL-L4420-2013-00012, To: Rich Deible, From: Andrew Duncan, Subject: Test Plan for Characterization and Analyses of Core Samples from C basin, September 16, 2013

[8] Specification 3019, Building Materials and Plumbing, Revision 28, E.I.duPont de Nemours & Company.

[9] Petrographic Investigation of Concrete from Building 221-H, Savannah River Site, U.S. Army Core of Engineers, 1996

[10] SRNS-STI-2008-00050, Evaluation of Sulfate Attack on Saltstone Vault Concrete and Saltstone, Part I: Final Report, August 2009.

[11] Carey, S.A., "Long Term Assessment of 105-P Structure for In-Situ D&D Alternatives," Savannah River Site, Aiken, SC, T-CLC-P-00004, August 2008

[12] Walton, J.C., Plansky, L.E., and Smith, R.W. (1990). "Models for Estimation of Service Life of Concrete Barriers in Low-Level Radioactive Waste Disposal". NUREG/CR-5542, September 1990.

[13] SRNL-STI-2010-00729, Evaluation of the Durability of the Structural Concrete of Reactor Buildings at SRS, A. J. Duncan and M. M. Reigel, December 2010

[14] *Manual for Inspecting, Evaluating, and Diagnosing Corrosion in Reinforced Concrete Structures*, Ibero-American Program Science and Technology for Development, (2000).

[15] SRNL technical reference procedure # SRNL-L29-ITS-0201, Rev. 4 "Analysis of Carbon and Sulfur in Pu Oxide Using the LECO CS-230 Carbon/Sulfur Determinator," 9/02/2014

[16] ASTM C 42 Test Method for Obtaining and Testing Drilled Cores and Sawed Beams of Concrete, ASTM, West Conshohocken, PA, 2013

[17] ASTM C1231 Practice for Use of Unbonded Caps in Determination of Compressive Strength of Hardened Concrete Cylinders, ASTM, West Conshohocken, PA, 2011

[18] Guidelines for Detection, Analysis, and Treatment of Materials-Related Distress in Concrete Pavements - Volume 3: Case Studies Using the Guidelines, L. L. Sutter, K. R. Peterson, T. J. Van Dam, K. D. Smith, M. J. Wade, Report # FHWA-RD-01- 165, August 2002

[19] ASTM C 150 Standard Specification for Portland Cement, ASTM, West Conshohocken, PA, 1999

[20] Guide to Evaluation of Strength Test Results of Concrete, ACI 214R-11, American Concrete Institute, April 2011.

[21] Shawn Carey, 105-L Process Building NPH Evaluation (U), T-CLC-L-00051, Rev. 3, 3/23/2005

[22] D. S. Neilson, NPH Evaluation 105-L Disassembly Basin, 12/10/ 2002

[23] Concrete Standard Engineering Specification SB 11U, "Joints (except floors on earth)" E. I. duPont de Nemours & Company, November 1966.

[24] SRS Site Procedure 7.2 Rev. 1, 3B Manual, "Guidance Related to Warehousing and Material Control," May 19, 1999.